International Journal of Chemical Studies

**P-ISSN: 2349-8528**
**E-ISSN: 2321-4902**
www.chemijournal.com
IJCS 2025; 13(3): 96-113
© 2025 IJCS
Received: 05-03-2025
Accepted: 07-04-2025

# In silico evaluation of Co(II), Mn(II), Cu(II), and Zn(II) complexes with hydrazide ligands: DFT, spectroscopic, and molecular docking studies

**Augustine Onuche Sule, Kehinde Gabriel Obiyenwa, Olalekan Wasiu Salawu and Banjo Semire**

**Augustine Onuche Sule**
Department of Chemistry, Federal University Lokoja, Kogi, Nigeria

**Kehinde Gabriel Obiyenwa**
Department of Chemistry, Federal University Lokoja, Kogi, Nigeria

**Olalekan Wasiu Salawu**
Department of Chemistry, Federal University Lokoja, Kogi, Nigeria

**Banjo Semire**
[1]Department of Chemistry, Federal University Lokoja, Kogi, Nigeria
[2]Computational Chemistry Research Laboratory, Department of Pure and Applied Chemistry, Ladoke Akintola University of Technology, Ogbomoso, Nigeria

**Corresponding Author:**
Banjo Semire
[1]Department of Chemistry, Federal University Lokoja, Kogi, Nigeria
[2]Computational Chemistry Research Laboratory, Department of Pure and Applied Chemistry, Ladoke Akintola University of Technology, Ogbomoso, Nigeria

**DOI:** https://www.doi.org/10.22271/chemi.2025.v13.i3b.12545

**Abstract**

This study explores the structural, electronic, spectroscopic, and antimicrobial properties of compounds containing hydrazide groups and their complexes with first-row transition metal ions. Hydrazides have potential applications in medicine, biological processes, and analytical chemistry. Quantum chemical methods and molecular docking were used to analyze the complexes with Isobutyrl acetic acid hydrazides (IBAH), 4-amino benzoic acid hydrazides (4-ABAH), and 4-cyano benzoic acid hydrazides (4-CBAH). The computational spectroscopic results align with experimental data. The metal complexes showed strong antibacterial properties against the crystal structure of Staph GyraseB 24kDa and *E. coli* GyraseB 24kDa, particularly the Cu(II)-4-CBAH (C7) and Cu(II)-4-ABAH (C10) complexes. The binding affinity and ADMET properties of these complexes are comparable to conventional antibiotics (ciprofloxacin and penicillin) and align with *in vitro* antibacterial performance against *E. coli* and *S. aureus*.

**Keywords:** Hydrazide complexes, DFT, molecular docking, antimicrobial activities

## Introduction

Creating new antimicrobial agents with distinct chemical properties compared to existing antibiotics and chemotherapeutic drugs is deemed essential to combat the increasing rates of antibiotic resistance (Rex *et al*., 2019) [1]. Therefore, it is necessary to explore novel compounds that exhibit significant antibacterial efficacy (Coates *et al*., 2011; Popiołek *et al*., 2018) [2,3]. Hydrazine, hydrazide, and their derivatives represent a promising class of compounds with noteworthy biological and pharmacological properties (Belkheiri *et al*., 2010)[4]. The primary activity associated with hydrazine and its hydrazide derivatives is their capability to scavenge free radicals. Additionally, researchers have examined the antibacterial and antifungal properties of these nitrogen-based compounds against various bacterial strains (Tolan *et al*., 2021) [5]. Hydrazides also play an essential role as chemotherapeutic agents in the treatment of tuberculosis (Tolan *et al*., 2021; Vicini *et al*., 2006) [5, 6]. Moreover, the hydrazide group has secured a significant position in medicinal chemistry as agents that exhibit antibacterial, antifungal, antitumor, anticonvulsant, anti-inflammatory, antimalarial, and antituberculosis activities (Ajani *et al*., 2010; Angelova *et al*., 2017; D. Kumar *et al*., 2012) [7-9].

Isonicotinic acid hydrazide (isoniazid; INH) is predominantly used as a primary medication for tuberculosis treatment and remains the most effective antituberculosis medicine, as endorsed by the WHO. Typically, conventional antibiotics target a single molecular site (Tolan *et al*., 2021; Manna & Agrawal, 2010) [5,10]. One strategy to address this limitation is to employ metal ions and their compounds as alternatives to traditional antibiotics (Soliman & Elsilk, 2018; Emam *et al*., 2020) [11, 12]. Metals are essential in biological redox reactions due to their capacity to exist in multiple oxidation states (Bagchi *et al*., 2015) [13]. Additionally, transition metal catalysts have become popular as useful tools in contemporary synthetic organic chemistry, owing to their varied reactivity that facilitates numerous chemical transformations (Takaya, 2021) [14]. Due to their different oxidation states, transition metals interact with specific negatively charged molecules (Monro *et al*., 2019) [15]. The combination of transition metals and organic moieties can be precisely designed for interactions with biological targets (Zhang & Sadler, 2017) [16]. Metal-containing compounds exhibit diverse mechanisms of action as antimicrobial agents. The chelation of organic compounds with metals results in significant modifications in the biological characteristics of both the metal and the ligand component (Emam *et al*., 2020; Joseph *et al*., 2013; Singh *et al*., 2011) [12, 17, 18]. The presence of metal complexes in biological frameworks forms the basis for the rapidly evolving field of bioinorganic chemistry.

Furthermore, the exploration of coordination compounds has permitted chemists to make notable progress in enhancing the understanding of chemical bonding concepts and the influence that bonding has on the varied properties of the compounds. Transition metal complexes, which generally include nitrogen, sulfur, or oxygen as ligand atoms, are becoming increasingly significant because they can interact with various metal centers through different coordination sites, allowing for the successful fabrication of metallic complexes with intriguing stereochemistry (Salawu *et al*., 2015) [19]. Hydrazide ligands represented by the general formula R-CO-NH-$NH_2$ have garnered attention in research due to their straightforward coordination capability with several transition metals at various active donor sites (C=O, NH, and $NH_2$). By inhibiting the -$NH_2$ group, the biological activity of the free ligand is enhanced. The antimicrobial effects of both hydrazides and their metal complexes are part of their captivating range of biological properties (Orhan Puskullu *et al*., 2013; Kumar *et al*., 2009; Narang *et al*., 2012) [20-22].

Nwambueze and Salawu (2012) synthesized complexes of Co(II), Mn(II), Cu(II), and Zn(II) with isobutryl acetic acid hydrazides (IBAH), 4-amino benzoic acid hydrazides (4-ABAH), and 4-cyano benzoic acid hydrazides (4-CBAH). These complexes were characterized by elemental analysis, IR and UV-visible spectra, and melting point/decomposition. Additionally, the potential geometry and coordination of these metals to the hydrazide ligands were investigated. The antibacterial properties of the complexes against *Staphylococcus aureus, Pseudomonas aeruginosa, Escherichia coli, and Klebsiella pneumonia* were also evaluated *in vitro* (Nwambueze & Salawu, 2012a, 2012b, 2012c) [23-25]. Although there is experimental evidence for these systems, little is known about their structure-activity correlations, especially about electronic properties and binding mechanisms, despite sophisticated spectroscopic techniques for clarifying these compounds' structures (Shevyrin *et al*., 2014) [26]. With advancements in computational technology and efficient computational methods, detailed quantum-chemical computations on molecular properties such as geometries, charge distributions, thermodynamic data, vibrational frequency, magnetic resonance parameters, and reaction pathways are now possible (Kirste, 2016) [27]. Previously, these methods were time-consuming and complicated. DFT calculations and molecular docking have been shown to accurately predict the vibrational frequencies, electronic spectra, and biological activities of metal complex molecules. DFT is also widely used to accurately calculate chemical shifts for diverse substances (Adekunle *et al*., 2015; Semire *et al*., 2017) [28,29]. This present work aims to provide insights into structural, electronic, spectroscopic, and anti-microbial activities of Co(II), Mn(II), Cu(II), and Zn(II) complexes with Isobutryl acetic acid hydrazides (IBAH), 4-amino benzoic acid hydrazides (4-ABAH) and 4-cyano benzoic acid hydrazides (4-CBAH) using Quantum chemical methods and molecular docking.

## Material and Methods

### Computational Details

The ligands (IBAH, 4-ABAH & 4-CBAH) and complexes (C1 to C12) were modeled and optimized using Spartan 2014v 1.1.4 software implemented on Dell Latitude 7480 computer system (Intel(R) Core (TM) i7-7600 CPU @2.8GHz/2.9GHz, 16GB RAM size on Microsoft Windows 11 Pro) based on the data obtained from the infrared spectra and elemental analysis of the complexes proposed from the literature (Nwambueze & Salawu, 2012a, 2012b, 2012c) [23-25] The complexes modeled structure consists of 6 coordinated $M^{2+}$ ($Co^{2+}$, $Mn^{2+}$, $Cu^{2+}$ and $Zn^{2+}$) complexes with two units of carbonyl oxygen bonded to the metal ion from the ligands, two nitrogen from the amino group and the other two units attaching to water molecules, thus giving six coordination around the metal ion giving an octahedral geometry as shown in Figure 1.

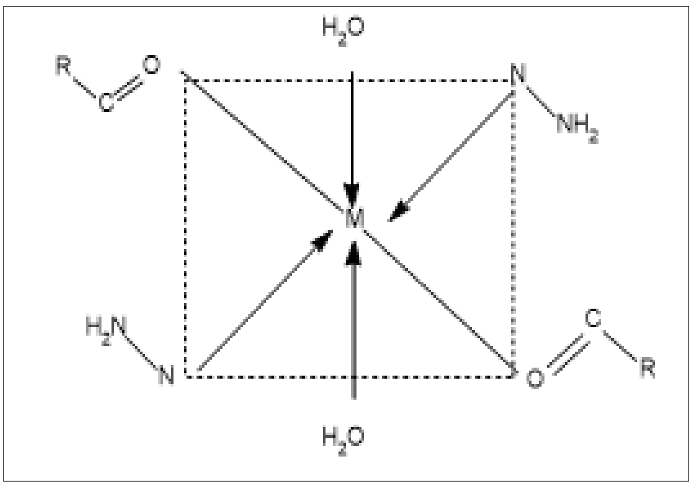


**Fig 1:** Proposed structure of the complexes showing Octahedral Geometry where M= $Co^{2+}$, $Mn^{2+}$, $Cu^{2+}$ and $Zn^{2+}$, and R=$(CH_3)_2CHC=OCH_2$, $C_6H_5CN$, $C_6H_4NH_2$.

Density Functional Theory (DFT) was used for the optimization of both ligands and complexes. DFT is a powerful tool for predicting the structure aspects and the relative stabilities of molecular systems. According to

Adekunle *et al*. (2016) and Demehin *et al*., (2020), the DFT level was based on the preliminary conformational search on all molecules using the MMFF method with the Monte Carlo search algorithm. DFT calculations were conducted using the hybrid B3LYP exchange and correlation functional and 6-31G** basis set, and all calculations were conducted without symmetry restriction (Paul *et al*., 2015) [30].

**Molecular Docking:** Molecular docking is an essential technique for determining the most favorable way for a molecule to bind to its target protein, considering both the target molecule (receptor) and the desired compounds (such as ligands and their metal chelates), with low binding free energy and high binding affinity (Abd El-Lateef *et al*., 2024) [31]. The *in vitro* antibacterial screening data against *Staphylococcus Aureus* and *Escherichia Coli* of the studied hydrazide ligands and their complexes from the literature (Nwambueze & Salawu 2012a, 2012b, 2012c) [23-25] is shown Table 1.

**Table 1:** Anti-Microbial Activity Results for Ligands and Complexes

| Compound | *E. coli* | *S.aureus* |
|---|---|---|
| IBAH | - | + |
| 4-CBAH | - | + |
| 4-ABAH | - | + |
| C1 (Co[IBAH]$_2$$^{2+}$ | + | -- |
| C2 (Cu[IBAH]$_2$$^{2+}$) | +++ | ++ |
| C3 (Zn[IBAH]$_2$$^{2+}$) | ++ | ++ |
| C4 (Mn[IBAH]$_2$$^{2+}$) | + | --- |
| C5(Mn[4-CBAH]$_2$$^{2+}$) | --- | + |
| C6 (Co[4-CBAH]$_2$$^{2+}$) | --- | --- |
| C7 (Cu[4-CBAH]$_2$$^{2+}$) | +++ | +++ |
| C8 (Zn[4-CBAH]$_2$$^{2+}$) | +++ | + |
| C9 (Zn[4-ABAH]$_2$$^{2+}$) | ++ | + |
| C10 (Cu[4-ABAH]$_2$$^{2+}$) | +++ | +++ |
| C11 (Co[4-ABAH]$_2$$^{2+}$) | --- | + |
| C12 (Mn[4-ABAH]$_2$$^{2+}$) | + | --- |

**Key:** High active = +++ (inhibition zone >12mm); moderately active = ++ (inhibition zone >9-12mm) slightly active = + (inhibition zone >6 - 9mm); Inactive = - - - (inhibition zone <6mm); *E. coli - Escherichia coli; S.aureus - Staphylococcus Aureus*.

To check for the binding affinity, selected metal complexes with biological activities against *Staphylococcus Aureus* and *Escherichia Coli* from the literature (Nwambueze & Salawu 2012a, 2012b, 2012c) [23-25]were used for the docking. Molecular Operating Environment (MOE) 2015.10 software is used to dock the selected metal complexes that exhibit antibacterial activities to a crystal structure of Staph GyraseB 24kDa in complex with Novobiocin (Pdb Id: 4URO) and Crystal Structure of *E. coli* GyraseB 24kDa in complex with 4-(4-bromo-1H-pyrazol-1-yl)-6-[(ethylcarbamoyl)amino]-N-(pyridine-3-yl) pyridine-3-carboxamide (Pdb Id: 6F86), all receptors downloaded from Protein Data Bank. Ciprofloxacin and penicillin are used as standard drugs. Before docking, the protein was meticulously prepared by removing solvents and co-ligands, adding hydrogen atoms, rectifying the chain, and identifying active areas (by redocking the crystalized ligands, comparing their active sites) (Shaaban, *et al*., 2023) [32]. The compounds under examination were optimized for docking by minimizing energy, adapting energy, calculating atomic charges, and assessing binding energy. This domain examined a variety of structural conformations to assess the stability of hydrogen bonds and van der Waals interactions. 10 conformers were chosen from a pool of 30 ligand-receptor poses based on their ability to accommodate the ligand molecule into the protein's active pocket and their positive scoring energy (Shaaban, *et al*., 2023) [33]. This comprehensive computational analysis shed light on the compounds' interactions and binding affinities with the target protein, providing vital information for understanding their therapeutic implications.

## Results and Discussion

**The Backbone Geometries of the Ligands and Their Complexes:** Optimization of C1(Co[IBAH]$_2$$^{2+}$), C2(Cu[IBAH]$_2$$^{2+}$), C3(Zn[IBAH]$_2$$^{2+}$), C4 (Mn[IBAH]22+), C5(Mn[4-CBAH]$_2$$^{2+}$), C6 (Co[4-CBAH]$_2$$^{2+}$), C7 (Cu[4-CBAH]$_2$$^{2+}$), C8(Zn[4-CBAH]$_2$$^{2+}$), C9 (Zn[4-ABAH]$_2$$^{2+}$), C10 (Cu[4-ABAH]$_2$$^{2+}$), C11(Co[4-ABAH]$_2$$^{2+}$) and C12(Mn[4-ABAH]$^{2+}$) complexes exhibit octahedral geometry around the Co(II), Cu(II), and Zn(II) centers, each attached to four atoms of oxygen (two from carbonyl groups and two from water molecules) and two nitrogen atoms (from the hydrazine moieties of the hydrazide ligands), creating a six-coordinate arrangement around the metal ions, as illustrated in Figure 2.

The interactions between metal ions and ligand sites in Co(II) complexes with IBAH, 4-CBAH, and 4-ABAH (C1, C6, and C11) show that Co-O2 (Co-O4) bonds measure 1.926 Å (1.917 Å), 2.063 Å (2.063 Å), and 2.009 Å (2.229 Å), respectively. For Co-O5 (Co-O6), the bond lengths are 1.933 Å (1.933 Å), 2.121 Å (2.121 Å), and 2.054 Å (2.073 Å), respectively. The distances for Co-N1 (Co-N3) are 2.598 Å (2.698 Å), 2.117 Å (2.117 Å), and 2.108 Å (2.356 Å), while the bond angles between the metal species and the ligand binding sites in the coordination sphere for the IBAH, 4-CBAH, and 4-ABAH complexes range from 54.16° to 178.53°, 62.77° to 180°, and 60° to 164.08°, respectively. In the case of Mn(II) complexes with IBAH, 4-CBAH, and 4-ABAH (C4, C5, and C12), the bond lengths Mn-O2 (Mn-O4) are measured at 2.018 Å (2.018 Å), 1.957 Å, and 2.032 Å (2.114 Å), respectively. The lengths for Mn-O5 (Mn-O6) are 2.139 Å (2.221 Å), 2.275 Å (2.275 Å), and 2.116 Å (2.166 Å), respectively. The distances for Mn-N1 (Mn-N3) are 2.112 Å (2.112 Å), 2.074 Å (2.074 Å), and 2.244 Å (3.434 Å), while the bond angles between the metal species and the binding sites in the coordination sphere for IBAH, 4-CBAH, and 4-ABAH complexes vary from 63.7° to 177.81°, 65.22° to 180°, and 38.99° to 164.55°, respectively.

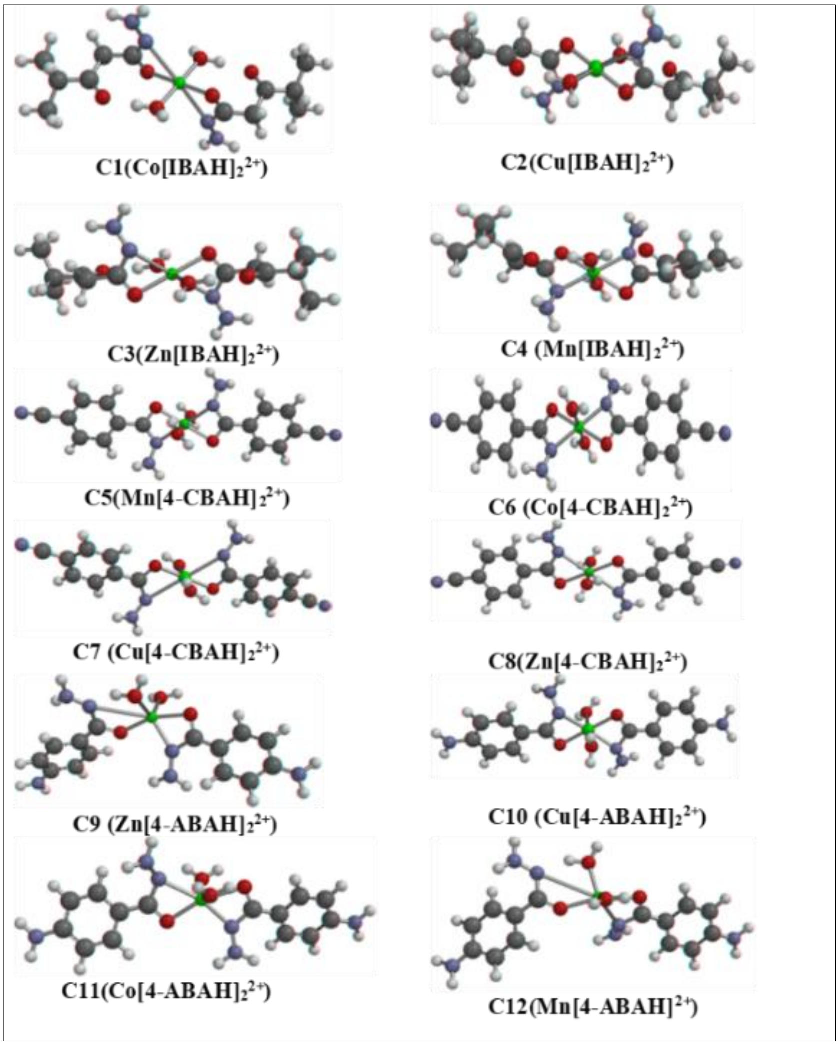


**Fig 2:** Optimized Structures of Complex (C1- C12) and Ligands.

For Cu(II) complexes with IBAH, 4-CBAH, and 4-ABAH (C2, C7, and C10), the bond lengths Cu-O2 (Cu-O4) are 1.943 Å (1.943 Å), 1.927 Å (1.927 Å), and 1.952 Å (1.943 Å), respectively. The lengths for Cu-O5 (Cu-O6) are 1.934 Å (1.934 Å), 1.992 Å (1.992 Å), and 2.279 Å (2.349 Å), respectively. The distances for Cu-N1 (Cu-N3) are 2.847 Å (2.847 Å), 2.669 Å (2.669 Å), and 2.110 Å (2.095 Å), while the bond angles between the metal species and the binding sites in the coordination sphere for IBAH, 4-CBAH, and 4-ABAH complexes range from 51.26° to 180°, 55.01° to 180°, and 65.27° to 179.33°, respectively. The bond lengths of Zn-O5 (Zn-O6) in Zn(II) complexes with IBAH, 4-CBAH, and 4-ABAH (C3, C8, and C9) measure 2.025 Å (2.025 Å) and 2.013 Å (2.070 Å) respectively; Zn-O2 (Zn-O4) exhibit values of 2.044 Å (2.044 Å), 2.004 Å (2.12 Å), and 1.970 Å (2.068 Å) respectively. The Zn-N1 (Zn-N3) bonds are recorded at 2.440 Å (2.440 Å), 2.341 Å, and 3.271 Å (2.142 Å) respectively, while the bond angles between the metal center and the binding sites within the coordination sphere for IBAH, 4-CBAH, and 4-ABAH complexes range from 58.02° to 180°, 60.26° to 180°, and 42.75° to 158.02° respectively. These measured bond lengths correspond well with those reported for similar six-coordinated structures in the literature (Alkurdi *et al*., 2022; Ramadan *et al*., 2021; Suleman & Al-Daher, 2023) [34-36]. During coordination, the bond angles formed within the hydrazide moiety of the ligands show variations, either increasing or decreasing, based on the bonding sequence. Nonetheless, the bond angles observed in the complexes fall within the expected range for octahedral geometry. This indicates that the bonding in these complexes likely involves hybridization patterns of $sp^3d^2$ or $d^2sp^3$ (Suleman & Al-Daher, 2023) [34].The calculated bond angles for complexes C1 to C12 are listed in Table 2.

**Table 2a:** Calculated geometrical parameters for C1 to C6

| C1 | | C2 | | C3 | | C4 | | C5 | | C6 | |
|---|---|---|---|---|---|---|---|---|---|---|---|
| **Bond Legth (Å)** | | | | | | | | | | | |
| Co-O2 | 1.926 | Cu-O2 | 1.943 | Zn-O2 | 2.044 | Mn-O2 | 2.018 | Mn-O1 | 1.957 | Co-O2 | 2.063 |
| Co-O4 | 1.917 | Cu-O4 | 1.943 | Zn-O4 | 2.044 | Mn-O4 | 2.018 | Mn-O2 | 1.957 | Co-O4 | 2.063 |
| Co-O5 | 1.933 | Cu-O5 | 1.934 | Zn-O5 | 2.025 | Mn-O5 | 2.139 | Mn-O5 | 2.275 | Co-O5 | 2.121 |
| Co-O6 | 1.933 | Cu-O6 | 1.934 | Zn-O6 | 2.025 | Mn-O6 | 2.221 | Mn-O6 | 2.275 | Co-O6 | 2.121 |
| Co-N1 | 2.598 | Cu-N1 | 2.847 | Zn-N1 | 2.44 | Mn-N1 | 2.112 | Mn-N1 | 2.074 | Co-N1 | 2.117 |
| Co-N3 | 2.698 | Cu-N3 | 2.847 | Zn-N3 | 2.44 | Nn-N3 | 2.112 | Mn-N3 | 2.074 | Co-N3 | 2.117 |
| BOND ANGLE (°) | | | | | | | | | | | |
| O2-Co-O4 | 178.53 | O2-Cu-O4 | 180 | O2-Zn-O4 | 180 | O2-Mn-O4 | 174.35 | O1-Mn-O2 | 180 | O2-Co-O4 | 180 |

| | | | | | | | | | | | |
|---|---|---|---|---|---|---|---|---|---|---|---|
| O2-Co-O5 | 92.86 | O2-Cu-O5 | 93.3 | O2-Zn-O5 | 94.37 | O2-Mn-O5 | 92.83 | O1-Mn-O5 | 92.05 | O2-Co-O5 | 90.98 |
| O2-Co-O6 | 86.80 | O2-Cu-O6 | 86.7 | O2-Zn-O6 | 85.63 | O2-Mn-O6 | 87.17 | O1-Mn-O6 | 87.95 | O2-Co-O6 | 89.02 |
| O2-Co-N1 | 56.04 | O2-Cu-N1 | 51.26 | O2-Zn-N1 | 121.98 | O2-Mn-N1 | 116.42 | O1-Mn-N1 | 114.78 | O2-Co-N1 | 62.77 |
| O2-Co-N3 | 127.31 | O2-Cu-N3 | 128.74 | O2-Zn-N3 | 58.02 | O2-Mn-N3 | 63.7 | O1-Mn-N3 | 65.22 | O2-Co-N3 | 117.23 |
| O4-Co-O5 | 87.06 | O4-Cu-O5 | 86.7 | O4-Zn-O5 | 85.63 | O4-Mn-O5 | 92.83 | O2-Mn-O5 | 87.95 | O4-Co-O5 | 89.02 |
| O4-Co-O6 | 93.32 | O4-Cu-O6 | 93.3 | O4-Zn-O6 | 94.37 | O4-Mn-O6 | 87.17 | O2-Mn-O6 | 92.05 | O4-Co-O6 | 90.98 |
| O4-Co-N1 | 122.49 | O4-Cu-N1 | 128.74 | O4-Zn-N1 | 58.02 | O4-Mn-N1 | 63.7 | O2-Mn-N1 | 65.22 | O4-Co-N1 | 117.23 |
| O4-Co-N3 | 54.16 | O4-Cu-N3 | 51.26 | O4-Zn-N3 | 121.98 | O4-Mn-N3 | 116.42 | O2-Mn-N3 | 114.78 | O4-Co-N3 | 62.77 |
| O5-Co-O6 | 178.51 | O5-Cu-O6 | 180 | O5-Zn-O6 | 180 | O5-Mn-O6 | 180 | O5-Mn-O6 | 180 | O5-Co-O6 | 180 |
| O5-Co-N1 | 93.13 | O5-Cu-N1 | 93.66 | O5-Zn-N1 | 86.22 | O5-Mn-N1 | 88.91 | O5-Mn-N1 | 92.9 | O5-Co-N1 | 87.89 |
| O5-Co-N3 | 86.3 | O5-Cu-N3 | 86.34 | O5-Zn-N3 | 93.78 | O5-Mn-N3 | 88.91 | O5-Mn-N3 | 87.1 | O5-Co-N3 | 92.11 |
| O6-Co-N1 | 87.88 | O6-Cu-N1 | 86.34 | O6-Zn-N1 | 93.78 | O6-Mn-N1 | 91.09 | O6-Mn-N1 | 87.1 | O6-Co-N1 | 92.11 |
| O6-Co-N3 | 92.75 | O6-Cu-N3 | 93.66 | O6-Zn-N3 | 86.22 | O6-Mn-N3 | 91.09 | O6-Mn-N3 | 92.9 | O6-Co-N3 | 87.89 |
| N1-Co-N3 | 176.61 | N1-Cu-N3 | 180 | N1-Zn-N3 | 180 | N1-Mn-N3 | 177.81 | N1-Mn-N3 | 180 | N1-Co-N3 | 180 |

**Table 2b:** Calculated geometrical parameters for C8 to C12.

| C7 | | C8 | | C9 | | C10 | | C11 | | C12 | |
|---|---|---|---|---|---|---|---|---|---|---|---|
| BOND LEGTH (Å) | | | | | | | | | | | |
| Cu-O2 | 1.927 | Zn-O1 | 2.004 | Zn-O2 | 1.97 | Cu-O2 | 1.952 | Co-O2 | 2.009 | Mn-O2 | 2.032 |
| Cu-O4 | 1.927 | Zn-O2 | 2.004 | Zn-O4 | 2.068 | Cu-O4 | 1.943 | Co-O4 | 2.229 | Mn-O4 | 2.114 |
| Cu-O5 | 1.992 | Zn-O3 | 2.121 | Zn-O5 | 2.013 | Cu-O5 | 2.279 | Co-O5 | 2.054 | Mn-O5 | 2.116 |
| Cu-O6 | 1.992 | Zn-O4 | 2.121 | Zn-O6 | 2.07 | Cu-O6 | 2.349 | Co-O6 | 2.073 | Mn-O6 | 2.166 |
| Cu-N1 | 2.669 | Zn-N3 | 2.341 | Zn-N1 | 3.271 | Cu-N1 | 2.11 | Co-N1 | 2.108 | Mn-N1 | 2.244 |
| Cu-N3 | 2.669 | Zn-N5 | 2.341 | Zn-N3 | 2.142 | Cu-N3 | 2.095 | Co-N3 | 2.356 | Nn-N3 | 3.434 |
| BOND ANGLE (°) | | | | | | | | | | | |
| O2-Cu-O4 | 180 | O1-Zn-O2 | 180 | O2-Zn-O4 | 158.02 | O2-Cu-O4 | 179.33 | O2-Co-O4 | 164.08 | O2-Mn-O4 | 164.55 |
| O2-Cu-O5 | 89.65 | O1-Zn-O3 | 91.01 | O2-Zn-O5 | 96.44 | O2-Cu-O5 | 87.28 | O2-Co-O5 | 106.01 | O2-Mn-O5 | 90.53 |
| O2-Cu-O6 | 90.35 | O1-Zn-O4 | 88.99 | O2-Zn-O6 | 99.41 | O2-Cu-O6 | 87.99 | O2-Co-O6 | 104.44 | O2-Mn-O6 | 98.52 |
| O2-Cu-N1 | 124.99 | O1-Zn-N3 | 119.74 | O2-Zn-N1 | 42.75 | O2-Cu-N1 | 115.37 | O2-Co-N1 | 103.93 | O2-Mn-N1 | 105.59 |
| O2-Cu-N3 | 55.01 | O1-Zn-N5 | 60.26 | O2-Zn-N3 | 97.26 | O2-Cu-N3 | 65.4 | O2-Co-N3 | 60 | O2-Mn-N3 | 38.99 |
| O4-Cu-O5 | 90.35 | O2-Zn-O3 | 88.99 | O4-Zn-O5 | 101.28 | O4-Cu-O5 | 92.48 | O4-Co-O5 | 79.73 | O4-Mn-O5 | 101.89 |
| O4-Cu-O6 | 89.65 | O2-Zn-O4 | 91.01 | O4-Zn-O6 | 85.18 | O4-Cu-O6 | 92.29 | O4-Co-O6 | 77.85 | O4-Mn-O6 | 84.31 |
| O4-Cu-N1 | 55.01 | O2-Zn-N3 | 60.26 | O4-Zn-N1 | 157.59 | O4-Cu-N1 | 65.27 | O4-Co-N1 | 60.26 | O4-Mn-N1 | 60.48 |
| O4-Cu-N3 | 124.99 | O2-Zn-N5 | 119.74 | O4-Zn-N3 | 62.54 | O4-Cu-N3 | 114.01 | O4-Co-N3 | 135.86 | O4-Mn-N3 | 154.52 |
| O5-Cu-O6 | 180 | O3-Zn-O4 | 180 | O5-Zn-O6 | 114.06 | O5-Cu-O6 | 173.76 | O5-Co-O6 | 140.41 | O5-Mn-O6 | 116.25 |
| O5-Cu-N1 | 87.7 | O3-Zn-N3 | 91.86 | O5-Zn-N1 | 56.46 | O5-Cu-N1 | 92.95 | O5-Co-N1 | 98.22 | O5-Mn-N1 | 118.12 |
| O5-Cu-N3 | 92.3 | O3-Zn-N5 | 88.14 | O5-Zn-N3 | 120.08 | O5-Cu-N3 | 98.28 | O5-Co-N3 | 85.49 | O5-Mn-N3 | 52.63 |
| O6-Cu-N1 | 92.3 | O4-Zn-N3 | 88.14 | O6-Zn-N1 | 100.98 | O6-Cu-N1 | 85.4 | O6-Co-N1 | 98.37 | O6-Mn-N1 | 119.42 |
| O6-Cu-N3 | 87.7 | O4-Zn-N5 | 91.86 | O6-Zn-N3 | 120.54 | O6-Cu-N3 | 83.43 | O6-Co-N3 | 88.36 | O6-Mn-N3 | 105.47 |
| N1-Cu-N3 | 180 | N3-Zn-N5 | 180 | N1-Zn-N3 | 128.16 | N1-Cu-N3 | 168.77 | N1-Co-N3 | 163.82 | N1-Mn-N3 | 127.92 |

**Frontier Molecular Orbitals and Global Reactivity Indices**

Understanding a molecule's electrical properties, reactivity, and chemical steadiness depends on its frontier molecular orbitals (FMOs), HOMO, and LUMO (El-Remaily *et al.*, 2023) [37]. Since the HOMO is the outermost (highest energy) orbital that contains electrons, it is the orbital energy that gives electrons. In contrast, the LUMO is the electron-accepting orbital, which is the lowest energy orbital that is the innermost (Semire *et al.*, 2017) [29]. Furthermore, the molecule's interactions with other species are controlled by its highest occupied and lowest unoccupied molecular orbitals, HOMO and LUMO, where HOMO functions as an electron donor and LUMO as an electron acceptor (Abdel-Rhman *et al.*, 2023; Latif *et al.*, 2023) [38,39]. HOMO-LUMO energies were used to determine the following: ionization potential (IP), energy gap (ΔE), electrophilicity index (ω), electronegativity (χ), chemical potentials (μ), global softness (δ), chemical hardness (η), and electron affinity (EA) (Mohapatra *et al.*, 2023) [40]. According to equations 1-7, these parameters were determined (Semire *et al.*, 2017; Hosny *et al.*, 2024) [29,41]:

$$\Delta E = LUMO - HOMO \quad (1)$$

$$-\chi = \mu = \frac{LUMO + HOMO}{2} \quad (2)$$

$$\eta = \frac{LUMO - HOMO}{2} \quad (3)$$

$$IP = -HOMO \quad (4)$$

$$EA = -LUMO \quad (5)$$

$$\delta = \frac{1}{\eta} \quad (6)$$

$$\omega = \frac{\chi^2}{8\eta} \quad (7)$$

Table 3 displays the optimized electronic characteristics (HOMO, LUMO, band gap, and dipole moment) determined at DFT/B3LYP/6-31G** in vacuum. For the complexes, the computed HOMO energies were as follows: -13.08 (C4) < -12.89 (C1) < -12.72 (C5) < -12.52 (C7) < -11.98 (C6) < -11.96 (C3) < -11.82 (C8) < -11.09 (C10) < -11.00 (C11) < -10.85 (C12) < -10.42 eV (C9). Additionally, the complexes' computed LUMO energies were in the following order: -11.35 (C3) < -11.28 (C8) < -11.20 (C6) < -10.59 (C4) < -10.26 (C5) < -9.98 (C9) < -9.87 (C7) < -9.38 (C2) < -8.89 (C11) < -8.72 (C12) < -8.52 (C10) < -8.26 eV (C1). The complex C9 has the highest HOMO energy, indicating its electron donation character, based on the HOMO-LUMO energy values. Furthermore, complex C1 has the highest energy value according to the LUMO data, indicating that it will take electrons from other species more easily than the other complexes. The HOMO and LUMO overlaid on the 12 complexes are shown in Figure 3.

The difference between HOMO and LUMO energies, referred to as band gap (ΔE), indicates the reactivity of the molecules. The molecule with a smaller ΔE responds better to docking (Abd El-Lateef et al., 2024) [31]. The modeled ligands' and complexes' calculated energy gaps rise in an orderly 0.44 (C9) < 0.54 (C8) < 0.61 (C3) < 0.78 (C6) < 2.11 (C11) < 2.13 (C12) < 2.46 (C5) < 2.49 (C4) < 2.57 (C10) < 2.65 (C7) < 3.42 (C2) < 4.63 eV (C1). And for the ligands, ΔE is as: 5.12 (4-ABAH) ≈ 5.13 (4-CBAH) < 5.74 eV (BAH). The calculated HOMO-LUMO energy gap shows that the ligands (IBAH, 4-CBAH and 4-ABAH) has the large values demonstrating their high stability, while their complexes exhibit small band gap values as a result of coordinating involving d-electrons. Lower ΔE for Zn(II) hydrazide complexes (C3,C8, and C9) revealing their reactivity and responsiveness to strong inter-electronic transitions or interactions with surrounding molecules; thus, higher binding affinities are expected with the protein receptors (Godwini *et al*., 2023) [42]. The electric dipole moment has been extensively used to describe the polarity and the interactions of a molecule in solvents (Kikuchi, 1987) [43], because it talks about the degree of polarity of a polar covalent bond. The computed dipole moments (in Debye) for the ligands and complexes are 2.86 (IBAH), 3.42 (4-CBAH), 4.62 (4-ABAH), 0.47 (C1), 0.01 (C2), 0.01 (C3), 5.23 (C4), 0.00 (C5), 0.02 (C6), 0.01 (C7), 0.00 (C8), 3.24 (C9), 3.18 (C10), 3.26 (C11) and 2.52 (C12). This indicates that complex C4 with higher dipole moment (5.23 Debye) is probably going to show stronger intermolecular interactions via ionic and polar interactions with the receptor, whereas complexes C5 and C8 with 0 dipole moments may show intramolecular attraction via van Der Waals force.

**Table 3:** Frontier orbital energies (eV) and dipole moment (DM, Debye) of the Ligands and Complex (C1-C12).

| Compound | Molecular Formula | HOMO (eV) | LUMO (eV) | (ΔE) (eV) | DM (Debye) |
|---|---|---|---|---|---|
| IBAH | $C_6H_{12}N_2O_2$ | -6.71 | -0.97 | 5.74 | 2.86 |
| 4-CBAH | $C_8H_7N_3O$ | -7.26 | -2.13 | 5.13 | 3.42 |
| 4-ABAH | $C_7H_9N_3O$ | -5.75 | -0.63 | 5.12 | 4.62 |
| C1 ($Co[IBAH]_2^{2+}$) | $C_{12}H_{26}CoN_4O_6$ | -12.89 | -8.26 | 4.63 | 0.47 |
| C2 ($Cu[IBAH]_2^{2+}$) | $C_{12}H_{26}CuN_4O_6$ | -12.80 | -9.38 | 3.42 | 0.01 |
| C3 ($Zn[IBAH]_2^{2+}$) | $C_{12}H_{26}ZnN_4O_6$ | -11.96 | -11.35 | 0.61 | 0.01 |
| C4 ($Mn[IBAH]_2^{2+}$) | $C_{12}H_{26}MnN_4O_6$ | -13.08 | -10.59 | 2.49 | 5.23 |
| C5 ($Mn[4\text{-}CBAH]_2^{2+}$) | $C_{16}H_{16}MnN_6O_4$ | -12.72 | -10.26 | 2.46 | 0.00 |
| C6 ($Co[4\text{-}CBAH]_2^{2+}$) | $C_{16}H_{16}CoN_6O_4$ | -11.98 | -11.20 | 0.78 | 0.02 |
| C7 ($Cu[4\text{-}CBAH]_2^{2+}$) | $C_{16}H_{16}CuN_6O_4$ | -12.52 | -9.87 | 2.65 | 0.01 |
| C8 ($Zn[4\text{-}CBAH]_2^{2+}$) | $C_{16}H_{16}ZnN_6O_4$ | -11.82 | -11.28 | 0.54 | 0.00 |
| C9 ($Zn[4\text{-}ABAH]_2^{2+}$) | $C_{14}H_{20}ZnN_6O_4$ | -10.42 | -9.98 | 0.44 | 3.24 |
| C10 ($Cu[4\text{-}ABAH]_2^{2+}$) | $C_{14}H_{20}CuN_6O_4$ | -11.09 | -8.52 | 2.57 | 3.18 |
| C11 ($Co[4\text{-}ABAH]_2^{2+}$) | $C_{14}H_{20}CoN_6O_4$ | -11.00 | -8.89 | 2.11 | 3.26 |
| C12 ($Mn[4\text{-}ABAH]_2^{2+}$) | $C_{14}H_{20}MnN_6O_4$ | -10.85 | -8.72 | 2.13 | 2.52 |

| Cpd | HOMO | LUMO | Cpd | HOMO | LUMO |
|---|---|---|---|---|---|
| C1 | 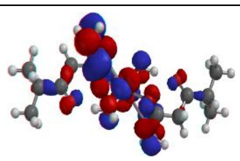 | 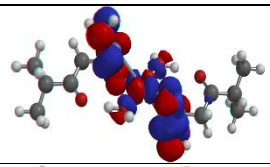 | C7 | 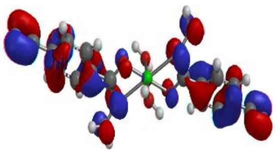 | 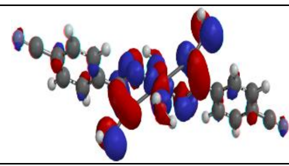 |
| C2 | 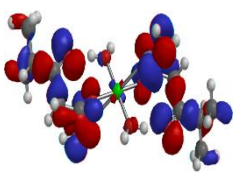 | 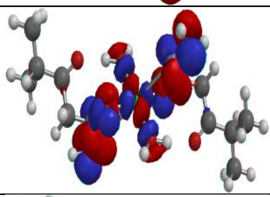 | C8 | 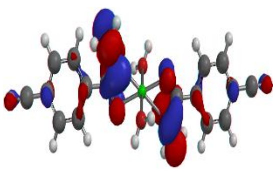 | 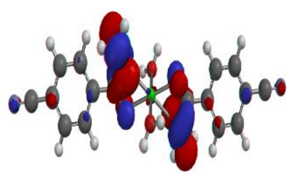 |
| C3 | 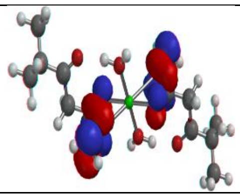 | 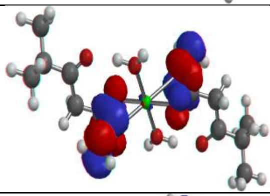 | C9 | 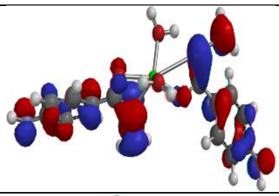 | 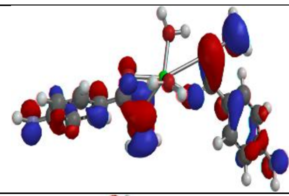 |
| C4 | 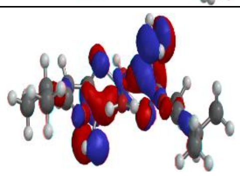 | 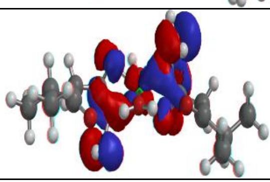 | C10 | 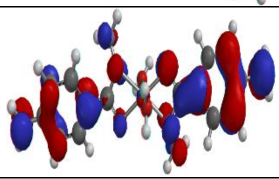 | 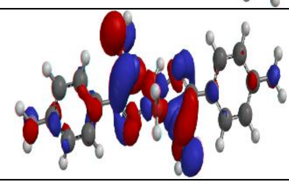 |

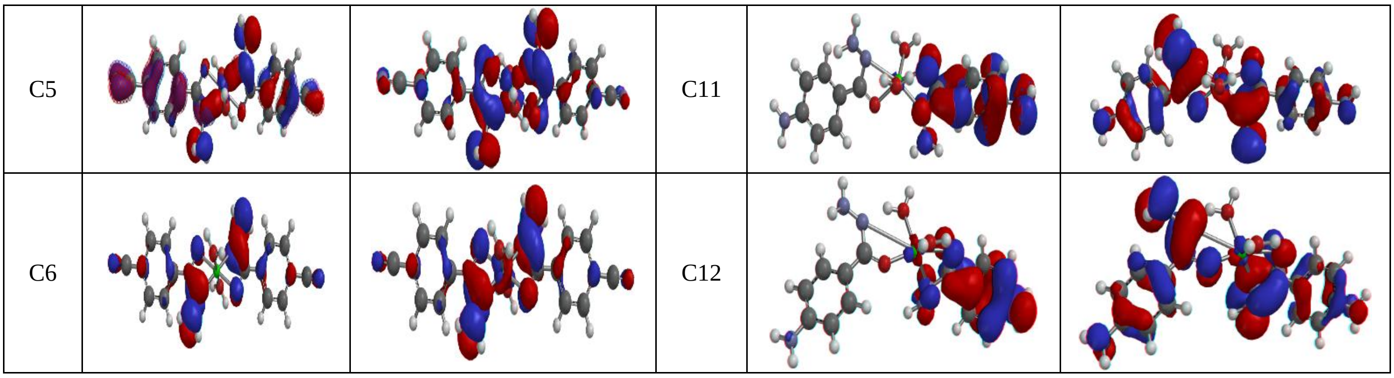


**Fig 3:** Frontier molecular orbitals: HOMO and LUMO of Complex (C1 to C12).

The global reactivity indices shown in Table 4 provide information about the stability and reactivity of the ligand and its complexes. Ionization Potential (IP) and electron affinity (EA) are energies required to extract and add an electron from a gaseous atom, respectively. Therefore, metals with low IP and ligands with higher EA tend to form more stable complexes, because metals with low IP can lose electrons more readily while ligands with higher EA can accept electrons more easily (Housecroft & Sharpe, 2008) [44]. Also, for ligands to serve as electrons' donors their EA values should be greater than their IP values; thus IBAH, 4-CBAH, 4-ABAH should be able to form stable complexes with metal ions in order: 4-ABAH < IBAH < 4-CBAH (Table 4). The ability of an atom to draw and retain electrons in a chemical bond is known as electronegativity. In essence, it indicates the strength with which an atom can attract electrons to itself while forming a chemical bond with another atom (Kikuchi, 1987; Pauling,1960) [43, 45], and higher electronegativity ligands tend to form more stable complexes because of stronger metal-ligand bonds (Chattaraj *et al*., 2011) [46]. The electronegativity ($\chi$) values are ordered as: 3.19 (4-ABAH) < 3.84 (IBAH) < 4.695 (4-CBAH) < 9.785 (C12) < 9.805 (C10) < 9.945 (C11) < 10.2 (C9) < 10.575 (C1) < 11.195 (C7) < 11.49 (C5) < 11.55 (C8) < 11.59 (C6) < 11.655 (C3) < 11.655 (C2) < 11.835 (C4). Consequently, higher $\chi$ value for C4 indicates its stability (Hosny *et al*., 2024) [41].

Two more important criteria that affect the global reactivity index are global softness ($\delta$) and chemical hardness ($\eta$). A molecule with a small HOMO-LUMO gap is said to be soft, meaning that it is easier to excite an electron from the HOMO to the LUMO (Chattaraj *et al*., 2011) [46], while chemical hardness ($\eta$) is the degree of resistance to alteration of the electronic density (Semire *et al*., 2017) [29]. Soft molecules could interact with biological compounds more readily than hard compounds; subsequently, biological activity rises with rising softness and falls with diminishing values of hardness (El-Remaily *et al*., 2023) [47]. Therefore, the order of reactivity could be: 0.348 (IBAH) < 0.390 (4-CBAH) < 0.391 (4-ABAH) < 0.432 (C1) < 0.585 (C2) < 0.755 (C7) < 0.778 (C10) < 0.803 (C4) < 0.813 (C5) < 0.939 (C12) < 0.948 (C11) < 2.564 (C6) < 3.279 (C3) < 3.704 (C8) < 4.545 (C9), indicating that the Zn(II) complexes (C9, C8 and C3) especially C9 are the most reactive complexes and are likely to interact with biological compounds more readily. The ability of a molecule to receive electrons is quantified by the global electrophilicity index ($\omega$). $\omega$ affects energy stabilization with metal surfaces or biological targets (Olanrewaju *et al*., 2023) [48]. A powerful electrophile that rapidly participates in processes as an electron acceptor is indicated by a high $\omega$ value (Chattaraj *et al*., 2011) [46]. The order of the ($\omega$) values is as follows: 0.497 (4-ABAH) < 0.642 (IBAH) < 1.074 (4-CBAH) < 6.038 (C1) < 9.352 (C10) < 9.930 (C2) < 11.238 (C12) < 11.823 (C7) < 13.043 (C11) < 13.417 (C5) < 14.063 (C4) < 43.054 (C6) < 55.672 (C3) < 59.114 (C9) < 61.760 (C8). The ligands have low $\omega$ values, so they can be classified as nucleophiles in a global electrophilicity index (Pérez *et al*., 2007) [49], while their complexes exhibit very strong electrophilicity index (higher $\omega$ values), indicating their electrophilic qualities, especially (C8, C9 and C3). This shows that the hydrazide complexes are reactive and electrophilic, making them suitable candidates for electron-accepting interaction in a biological environment and promising drug candidates (Olanrewaju *et al*., 2023) [48]

**Table 4:** The global reactivity indices (eV) of the Ligand and Complex (C1 to C12).

| Compounds | IP | EA | $\eta$ | $\mu$ | $\chi$ | $\delta$ ($eV^{-1}$) | $\omega$ |
|---|---|---|---|---|---|---|---|
| IBAH | 5.74 | 6.71 | 2.870 | -3.840 | 3.840 | 3.840 | 0.348 |
| 4-CBAH | 5.13 | 7.26 | 2.565 | -4.695 | 4.695 | 4.695 | 0.381 |
| 4-ABAH | 5.12 | 5.75 | 2.560 | -3.190 | 3.190 | 3.190 | 0.391 |
| C1 | 12.89 | 8.26 | 2.315 | -10.575 | 10.575 | 0.432 | 6.038 |
| C2 | 12.80 | 9.38 | 1.710 | -11.655 | 11.655 | 0.585 | 9.930 |
| C3 | 11.96 | 11.35 | 0.305 | -11.655 | 11.655 | 3.279 | 55.672 |
| C4 | 13.08 | 10.59 | 1.245 | -11.835 | 11.835 | 0.803 | 14.063 |
| C5 | 12.72 | 10.26 | 1.230 | -11.490 | 11.490 | 0.813 | 13.417 |
| C6 | 11.98 | 11.2 | 0.390 | -11.590 | 11.590 | 2.564 | 43.054 |
| C7 | 12.52 | 9.87 | 1.325 | -11.195 | 11.195 | 0.755 | 11.823 |
| C8 | 11.82 | 11.28 | 0.270 | -11.550 | 11.550 | 3.704 | 61.760 |
| C9 | 10.42 | 9.98 | 0.220 | -10.200 | 10.200 | 4.545 | 59.114 |

| | | | | | | | |
|---|---|---|---|---|---|---|---|
| C10 | 11.09 | 8.52 | 1.285 | -9.805 | 9.805 | 0.778 | 9.351 |
| C11 | 11.00 | 8.89 | 1.055 | -9.945 | 9.945 | 0.948 | 13.043 |
| C12 | 10.85 | 8.72 | 1.065 | -9.785 | 9.785 | 0.939 | 11.238 |

**Vibrational Frequencies**

Vibrational spectroscopy is a fundamental technique used in structural elucidation, particularly in finding functional groups and separating molecular conformers and isomers of molecules (Semire *et al.*, 2017) [29]. A comparison of experimental and theoretical vibrational modes, with proper assignment, could help understand a pretty complex system. Computed quantum chemical harmonic vibrational frequencies are usually greater than the basics seen empirically, due to the anharmonic nature of the potential energy curve of molecules in reality (Merrick *et al*., 2007) [50]. One of the main causes of this dispute is the theoretical treatment's disregard for anharmonicity consequences. Additionally, errors occur due to the usage of finite basis sets and the inadequate inclusion of electron correlation (Bello and Semire, 2013) [51]. The use of generic frequency scale factors (λ) is made possible by the comparatively uniform overestimation of quantum chemical harmonic vibrational frequencies for a given theoretical approach. For DFT at the B3LYP/6-31G** basis set, the scaling factor (λ) is 0.9623 (Merrick *et al*., 2007) [50]. Table 6 shows the observed experimental vibrational frequencies from the literature (Nwambueze & Salawu, 2012a, 2012b, 2012c) [23-25], computed and scaled (at B3LYP/6-31G**) vibrational frequencies for ligands and complexes.

The infrared spectra bands (Table 9) were assigned by critically comparing the spectra of the free ligand (IBAH, 4-CBAH, and 4-ABAH) with those of the complexes. Three major vibrations have been used successfully to infer the coordination of ligands to the metal in the spectra of complexes of hydrazides. These are the carbonyl stretching frequency [*v*(C=O)] or the “amide I”, the in-plane bending deformation and stretching frequency for cyanate [δ(N-H) and v(C-N)] or the” amide II” and the amino stretching vibrations *v*($NH_2$) (Adekunle *et al*., 2013) [52]. The amino group band *v*($NH_2$) was calculated (using DFT at B3LYP/6-31G**) and scaled to be in region 3796-3458, 3484-3316, and 3480-3306 $cm^{-1}$ for IBAH, 4-CBAH and 4-ABAH respectively. Experimentally, these bands were observed at 3855-3460, 3281, and 3420-3466 $cm^{-1}$ for IBAH, 4-CBAH, and 4-ABAH, respectively. The experimental (scaled-calculated) spectra show that these bands shifted to lower wavenumber in all complexes i.e. 3450-3050 $cm^{-1}$ (3529- 3231 $cm^{-1}$) (Nwambueze & Salawu, 2012a, 2012b, 2012c) [23-25]. This indicates the coordination of the metal ion to the amino group. Similarly, the “amide I” band [i.e. *v*(C=O)] was observed experimentally at 1666, 1631, and 1608 $cm^{-1}$ for IBAH, 4-CBAH, and 4-ABAH respectively was lowered to 1650 to 1620 $cm^{-1}$ upon coordination indicating the ligands are coordinated (Nwambueze & Salawu, 2012a, 2012b, 2012c) [23-25] Through the carbonyl oxygen. These bands were found at 1691-1646 $cm^{-1}$ for IBAH, 1619 $cm^{-1}$ for 4-CBAH, and 1618 $cm^{-1}$ for 4-ABAH for DFT calculations which shifted to 1641-1606 $cm^{-1}$ on coordination to metal ion of the complexes (Adekunle *et al*., 2013) [52]. The "amide II" band was observed experimentally in 1528, 1561, and 1506 $cm^{-1}$ for IBAH, 4-CBAH, and 4-ABAH, respectively. This band was found at 1555 $cm^{-1}$ for IBAH, 1586 $cm^{-1}$ for 4-CBAH, and 1534 $cm^{-1}$ for 4-ABAH for DFT calculations. This band also experienced a bathochromic shift in coordination to central metal ion observed around 1570-1450 $cm^{-1}$ for the complexes. The calculated 'amide II' for the complexes was at 1539-1461 $cm^{-1}$ for DFT (Nwambueze & Salawu 2012a, 2012b, 2012c; Adekunle *et al*., 2013) [23-25, 52].

The broadband in the region 3034-3740$cm^{-1}$ and 3256-3730$cm^{-1}$ observed experimentally and calculated respectively is accorded to v(O-H) stretching vibration, a feature indicating the presence of water. Bands around this region can also be assigned to $v_s$(OH) of water molecules of hydrogen. This band is also supported by an additional band appearing in the range 890-750 $cm^{-1}$ attributed to vibration of the v(O-H) bond, indicating the presence of water molecule, or confirming the presence of lattice-held water molecule in the complexes. This water molecule could be a lattice or coordinated (Nwambueze & Salawu, 2012a, 2012b, 2012c) [23-25].

The nature of the metal-ligand bonding observed experimentally (calculated by DFT) by newly formed bands 300-400 (318- 434) $cm^{-1}$ and 300-550 (436- 538) $cm^{-1}$ is assigned to the metal-nitrogen (M-N) and metal to oxygen (M-O) vibrations respectively (Nwambueze & Salawu, 2012a, 2012b, 2012c) [23-25]. The vibrational frequencies scaled calculated at DFT are closer to the experimentally determined values indicating that the scaled vibrational frequencies are in agreement with the experimental observation.

**Table 6:** Some selected experimental and calculated (B3LYP/6-31G**) Vibrational Frequencies for the Ligands and complexes.

| *v*(OH) | | | | AMIDE I *v*(C-O, C=O) | | | *v*($NH_2$/NH) | | | AMIDE II *v*(C-N) | | | *v*(M-N) | | | *v*(M-O) | | |
|---|---|---|---|---|---|---|---|---|---|---|---|---|---|---|---|---|---|---|
| S/N | Exp. | Cal. | Scaled | Exp. | Cal. | Scaled | Exp. | Cal. | Scaled | Exp. | Cal. | Scaled | Exp. | Cal. | Scaled | Exp. | Cal. | Scaled |
| IBAH | | | | 1666 | 1710 1756 | 1646 1691 | 3855 3460 | 3943 3974 3592 | 3796 3826 3458 | 1528 | 1615 | 1555 | | | | | | |
| 4-CBAH | | | | 1631 | 1682 | 1619 | 3281 | 3444 3516 3619 | 3316 3385 3484 | 1561 | 1647 | 1586 | | | | | | |
| 4-ABAH | | | | 1608 | 1681 | 1618 | 3420 3466 | 3434 3506 3615 | 3306 3375 3480 | 1506 | 1593 | 1534 | | | | | | |
| C1 | 3450 | 3556 3657 | 3423 3521 | 1630 | 1702 | 1639 | 3200 3300 | 3485 3486 3648 | 3355 3356 3512 | 1486 | 1523 | 1466 | 420 | 440 | 424 | 488 | 510 | 491 |
| C2 | 3350 | 3570 | 3437 | 1620 | 1700 | 1637 | 3220 3440 | 3480 3643 3613 | 3350 3507 3478 | 1487 | 1524 | 1467 | 395 | 409 | 394 | 480 | 498 | 479 |
| C3 | 3500 | 3667 | 3530 | 1625 | 1693 | 1630 | 3250 | 3386 | 3260 | 1456 | 1513 | 1457 | 400 | 430 | 414 | 488 | 509 | 490 |

| | | | | | | | | | | | | | | | | | | |
|---|---|---|---|---|---|---|---|---|---|---|---|---|---|---|---|---|---|---|
| | | 3382 | 3256 | | | | | 3496<br>3652<br>3653 | 3366<br>3516<br>3517 | | | | | | | | | |
| C4 | 3560 | 3700<br>3795 | 3562<br>3653 | 1640 | 1705 | 1641 | 3260 | 3356<br>3463 | 3231<br>3334 | 1470 | 1546<br>1561 | 1488<br>1503 | 360 | 351 | 338 | 489 | 559 | 538 |
| C5 | 3400 | 3548<br>3874 | 3416<br>3730 | 1650 | 1678 | 1615 | 3420 | 3479<br>3580<br>3664 | 3349<br>3446<br>3527 | 1573 | 1569 | 1510 | 380 | 400 | 385 | 478 | 489 | 471 |
| C6 | 3500 | 3681<br>3592 | 3544<br>3458 | 1640 | 1675 | 1613 | 3400 | 3491<br>3497<br>3617<br>3668 | 3361<br>3367<br>3482<br>3531 | 1456 | 1586<br>1577 | 1527<br>1518 | 330 | 338 | 325 | 499 | 540 | 520 |
| C7 | 3350 | 3520<br>3581 | 3389<br>3447 | 1620 | 1687 | 1624 | 3400,<br>3300 | 3464<br>3565<br>3646 | 3335<br>3432<br>3510 | 1573 | 1596<br>1596 | 1536<br>1536 | 305 | 330 | 318 | 490 | 527 | 507 |
| C8 | 3450 | 3622<br>3793 | 3487<br>3652 | 1630 | 1677 | 1614 | 3430 | 3475<br>3483<br>3600<br>3659 | 3345<br>3353<br>3466<br>3523 | 1566 | 1599 | 1539 | 420 | 425 | 409 | 468 | 494 | 476 |
| C9 | 3452 | 3613<br>3868 | 3652<br>3724 | 1640 | 1677 | 1614 | 3100,<br>3450 | 3610<br>3672 | 3475<br>3535 | 1550 | 1590 | 1531 | 400 | 442 | 426 | 490 | 532 | 512 |
| C10 | 3450 | 3616<br>3807 | 3481<br>3665 | 1625 | 1655 | 1593 | 3050, | 3496<br>3499<br>3596<br>3597 | 3366<br>3368<br>3462<br>3463 | 1450 | 1518<br>1519 | 1461<br>1462 | 310 | 350 | 337 | 450 | 453 | 436 |
| C11 | 3500 | 3669<br>3681 | 3532<br>3544 | 1650 | 1676 | 1613 | 3100 | 3489<br>3499<br>3598<br>3599 | 3359<br>3369<br>3464<br>3465 | 1477 | 1515<br>1534 | 1458<br>1477 | 410 | 428 | 412 | 500 | 531 | 511 |
| C12 | | 3353<br>3793 | 3228<br>3652 | 1655 | 1668 | 1606 | 3100 | 3491<br>3496<br>3600<br>3666 | 3361<br>3366<br>3466<br>3529 | 1570 | 1592<br>1591 | 1533<br>1532 | 400 | 451 | 434 | 490 | 519 | 500 |

## Electronic Spectra

Electronic spectra are used to determine the stereochemistry of metal complexes based on the position and number of d→d transition peaks. Absorption spectra can be extremely useful in evaluating the results of other structural inquiry methods (Nwambueze & Salawu, 2012a, 2012b, 2012c) [23-25]. Using the TD-DFT/6-31G** level of theory, the molecular orbital (MO) corresponding to each electronic transition is checked to acquire minute information on the electronic transitions (Semire *et al*., 2017) [29] The diamagnetic Zn(II) complexes do not exhibit any characteristics of d-d transitions. The experimental in agreement with (theoretical) electronic spectra of Zn (II) complexes of C3, C8, and C9 exhibit a high-intensity band at 28680 (25451.12 $cm^{-1}$), 28350 (26989.10 $cm^{-1}$) and 28445 (27482.34 $cm^{-1}$), respectively (Table 7), and are assigned to charged transfer. However, in analogy of those described for Zn(II) complexes containing N-O donor hydrazides from literature and according to empirical formulae of these complexes an octahedral geometry can be proposed for the complexes (Nwambueze & Salawu, 2012a, 2012b, 2012c) [23-25]. The electronic spectra of Cu(II) complexes of C2, C7, and C10 show single d→d bands located at 15168 (14283.27 $cm^{-1}$), 15385 (15620.36 $cm^{-1}$) and 13006 (12908.56$cm^{-1}$), respectively (Table 7), which are consistent for an octahedral geometry. In octahedral complexes of Co(II), three transitions namely ${}^4T_{1g}(F)\rightarrow{}^4T_{1g}(P)$, ${}^4T_{1g}(F)\rightarrow{}^4A_{2g}(F)$ and ${}^4T_{1g}(F)\rightarrow{}^4T_{2g}(F)$ are possible. The electronic spectra of Co(II) complexes of C1, C6 and C11 shows band at 23250 (21934.15 $cm^{-1}$), 24690 (23112.30 $cm^{-1}$) and 15540 (15450.46$cm^{-1}$) respectively and are assigned to ${}^4T_{1g}(F)\rightarrow{}^4T_{1g}(P)$ transition and bands at 19300 and 18690 $cm^{-1}$ for C1 and C6 respectively assigned to ${}^4T_{1g}(F)\rightarrow{}^4A_{2g}(F)$ transition. It is well known that the d-d transition occurs in $d^5$ systems but these transitions are of very low intensities (Nwambueze & Salawu, 2012a) [23]. The experimental electronic spectra for Mn(II) complexes of C4, C5, and C12 indicated the presence of three weak peaks at 19531, 22883 and 26101 $cm^{-1}$ which may be assigned to ${}^6A_{1g}\rightarrow{}^4T_{1g}(4G)$, ${}^6A_{1g}\rightarrow{}^4E_g(4G)$, ${}^6A_{1g}\rightarrow{}^4E_g(4D)$ transitions, respectively, signifying that the Mn(II) complex has octahedral geometry which correspond to the calculated electronic spectra showing peaks at 18371.88 $cm^{-1}$ assigned to ${}^6A_{1g}\rightarrow{}^4T_{1g}(4G)$ for C4, 18734.31 $cm^{-1}$ also assigned to ${}^6A_{1g}\rightarrow{}^4T_{1g}(4G)$ for C5, 18845.52 and 21575.44 $cm^{-1}$ assigned to ${}^6A_{1g}\rightarrow{}^4T_{1g}(4G)$ and ${}^6A_{1g}\rightarrow{}^4E_g(4G)$, respectively, signifying that the Mn(II) complex has octahedral geometry (Shakdofa *et al*., 2021) [53].

**Table 7:** Selected Observed Experimental, calculated (at B3LYP/6-31G**) Electronic Spectral data for the Complexes.

| S/N | Λ $cm^{-1}$ Cal. | Λ $cm^{-1}$ Exp. | Assignment |
|---|---|---|---|
| C1 | 21934.15 | 23250,<br>19300 | ${}^4T_1g(F)\rightarrow{}^4T_1g(P)$,<br>4T1g(F)→4A2g |
| C2 | 14283.27 | 15168 | d→d |
| C3 | 25451.12 | 28680 | CT |
| C4 | 18371.88 | 19531,<br>22883,<br>26101 | ${}^6A_{1g}\rightarrow{}^4T_{1g}(4G)$,<br>${}^6A_{1g}\rightarrow{}^4E_g(4G)$,<br>${}^6A_{1g}\rightarrow{}^4E_g(4D)$ |
| C5 | 18734.31 | 19531,<br>22883,<br>26101 | ${}^6A_{1g}\rightarrow{}^4T_{1g}(4G)$,<br>${}^6A_{1g}\rightarrow{}^4E_g(4G)$,<br>${}^6A_{1g}\rightarrow{}^4E_g(4D)$ |
| C6 | 23112.30 | 24690, | ${}^4T_1g(F)\rightarrow{}^4T_1g(P)$, |

| | | | |
|---|---|---|---|
| | | 18690 | $^4T_1g(F)\rightarrow{}^4A_2g$ |
| C7 | 15620.36 | 15385 | d→d |
| C8 | 26989.10 | 28350 | CT |
| C9 | 27482.34 | 28445 | CT |
| C10 | 12908.56 | 13006 | d→d |
| C11 | 15450.46 | 15540 | $^4A_2g\rightarrow{}^4T_1g(P)$ |
| C12 | 18845.52,<br>21575.44 | 19531,<br>22883,<br>26101 | $^6A_{1g}\rightarrow{}^4T_{1g}(4G)$,<br>$^6A_{1g}\rightarrow{}^4E_g(4G)$,<br>$^6A_{1g}\rightarrow{}^4E_g(4D)$ |

**Mulliken Charge**

One of the most useful techniques for calculating the charge population distributions of a molecule in quantum chemistry is Mulliken charge (Semire *et al*., 2017) [29]. The electronic charges (electron density) on the chosen heteroatoms can give information on changes in vibrational spectrum, which in turn affects many other aspects of the system, such as the atoms' bond lengths, dipole moments, electronic structures, molecule polarizability, and acidity-basicity properties (Preethi *et al*., 2024) [54]. Also, many chemical reactions and the physico-chemical characteristics of substances depend on the electron densities (Semire *et al*., 2017) [29]. The data obtained by Mulliken analysis showed that all complex metal ions possess positive charges and act as electron donors. The Mulliken charge of the complexes metal ion are ordered as: $Cu^{2+}$ — C10, C7 and C2 (0.908, 0.973 and 0.983, respectively) < $Zn^{2+}$ — C8, C9 and C3 (1.006, 1.009 and 1.033, respectively) < $Co^{2+}$- C1, C6 and C11 (1.009, 1.090 and 1.057, respectively) < $Mn^{2+}$ — C12, C5 and C4 (1.202, 1.301 and 1.307, respectively) as shown in Table 8, which suggest that lower positive Mulliken charges on the $Cu^{2+}$ ion reveal that $Cu^{2+}$ ion donate more electrons to the ligands through M-ligand bonding, which result into shorter Cu-O in the Cu(II) complexes than other M(II) complexes (Tables 1 and 2). The high negative oxygen Mulliken charges on Oxygen atoms (O1, O2, O3, O4, O5, and O6) and nitrogen atoms (N1, N3, and N5) indicting high centers for coordination by accepting electrons from $M^{2+}$ ion.

**Table 8:** Mulliken Charges of The C1 to C12 complex at B3LYP/6-31G** basis set.

| S/N | M | O1 | O2 | O3 | O4 | O5 | O6 | N1 | N3 | N5 |
|---|---|---|---|---|---|---|---|---|---|---|
| C1 | 1.009 | | -0.650 | | 0.634 | -0.629 | -0.600 | -0.370 | -0.465 | |
| C2 | 0.983 | | -0.535 | | -0.525 | -0.655 | -0.655 | -0.276 | -0.276 | |
| C3 | 1.033 | | -0.514 | | -0.514 | -0.654 | -0.654 | -0.321 | -0.321 | |
| C4 | 1.307 | | -0.564 | | -0.564 | -0.709 | -0.629 | -0.441 | -0.441 | |
| C5 | 1.301 | -0.639 | -0.639 | | | -0.63 | -0.63 | -0.503 | -0.503 | |
| C6 | 1.09 | | -0.589 | | -0.589 | -0.612 | -0.612 | -0.437 | -0.437 | |
| C7 | 0.973 | | -0.593 | | -0.593 | -0.599 | -0.599 | -0.327 | -0.327 | |
| C8 | 1.006 | -0.586 | -0.586 | -0.603 | -0.603 | | | | -0.369 | -0.369 |
| C9 | 1.009 | | -0.65 | | -0.632 | -0.626 | -0.6 | -0.37 | -0.465 | |
| C10 | 0.908 | | -0.602 | | -0.604 | -0.594 | -0.587 | -0.423 | -0.425 | |
| C11 | 1.057 | | -0.613 | | -0.615 | -0.608 | -0.609 | -0.465 | -0.415 | |
| C12 | 1.202 | | -0.679 | | -0.642 | -0.672 | -0.634 | -0.465 | -0.383 | |

**Molecular Docking**

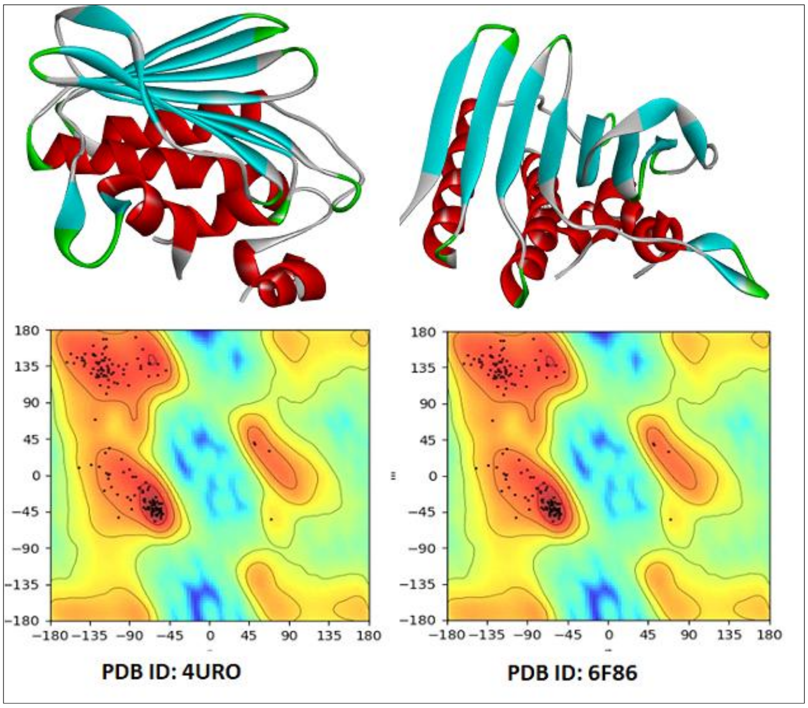


**Fig 4:** crystal structure of the receptors (4URO and 6F86) with their Ramachandran plots

One of the most crucial techniques for predicting the possibility for restriction and interaction manner also mechanical details of biochemical moiety in enzyme's sector is molecular docking modeling (Elkanzi *et al*., 2023) [55]. The crystal structures of the *S. aereus* (Staph GyraseB 24kDa in complex with Novobiocin with Pdb Id: 4URO) and *E.coli* (GyraseB 24kDa in complex with 4-(4-bromo-1H-pyrazol-1-yl)-6-[(ethylcarbamoyl)amino]-N-(pyridine-3-yl)pyridine-3-carboxamide with Pdb Id: 6F86) were from the protein data bank (http://www.rcsb.org/pdb) as shown in Figure 4. All heteroatoms, water molecules and other unwanted materials were removed from the downloaded protein using Pymol v1,7.4.4 and Discovery Studio software v.2019. The Ramachandran plot showed that both receptors are of good quality with VADAR webserver. 89% (91%) of the amino acids are in the most favorable region, 9% (7%) are in the unfavorable region, and 2% (2%) of the amino acids are disallowed or forbidden for 4URO (6F86). Molecular Operating Environment (MOE, 2015.10) tool was used to dock the complexes C2, C3, C7, C8, C9, C10 chosen as a result of their activities against *S. aereus* (Staph GyraseB 24kDa in complex with Novobiocin with Pdb Id: 4URO) and *E.coli* (GyraseB 24kDa in complex with 4-(4-bromo-1H-pyrazol-1-yl)-6-[(ethylcarbamoyl)amino]-N-(pyridine-3-yl)pyridine-3-carboxamide with Pdb Id: 6F86).

For the 6F86, the docking result shows that the binding energy (BE) is between -5.977 and -5.054 kcal/mol with C7 and C10 having highest binding affinities of -5.433 and -5.977 kcal/mol, respectively. The BE for standard drugs are -5.678 and -5.885 kcal/mol for Ciprofloxacin and Penicillin, respectively (Table 8). Although the BE of the standard drugs are higher than of C7 and C10, the BE of these two complexes are in agreement with strong inhibitions of C7 and C10 against *E.coli* as observed experimentally (Table 1). The pronounced electrophilicity and a large HOMO-LUMO energy gap (means high stability) may also play a crucial role in the interactions of the two complexes with the 6F86 receptor (Wahab *et al*., 2022) [56]. The C7 interacts via carbonyl oxygen of GLUA50 and oxygen of one of the water ligand (metal/ion contact), cyano nitrogen of ARGB136, amino nitrogen of ASPA49 and ASNA46 with second water oxygen atom through hydrogen bonding (Figure 5). C10 interacts with GLUA50 via the carbonyl oxygen and coordinated water oxygen atom both via hydrogen bonding. Ciprofloxacin interacts with ASPA73 with the enone carbon and carbonyl oxygen of the enone group through hydrogen bonding, while penicillin interacts with GLUA50 of thiazolidine sulfur and ASNA48 with side chain amide nitrogen via hydrogen bonding of 6F86 receptor.

**Table 9:** Binding affinities of the docked Metal complexes and standard drugs (Ciprofloxacin and Penicillin) with different bacterial receptors.

| Molecule | Binding affinity (Kcal/mol) for 6F86 | Binding affinity (Kcal/mol) for 4URO |
|---|---|---|
| C2 | -5.081 | -5.077 |
| C3 | -5.251 | -5.160 |
| C7 | -5.433 | -5.811 |
| C8 | -5.139 | -5.510 |
| C9 | -5.054 | -4.790 |
| C10 | -5.977 | -5.519 |
| Ciprofloxacin | -5.678 | -5.858 |
| Penicillin | -5.885 | -5.901 |

| Molecule | 2-D | 3-D |
|---|---|---|
| C2 | 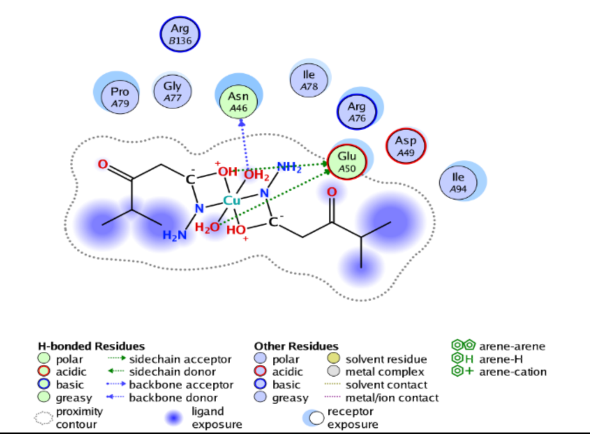 | 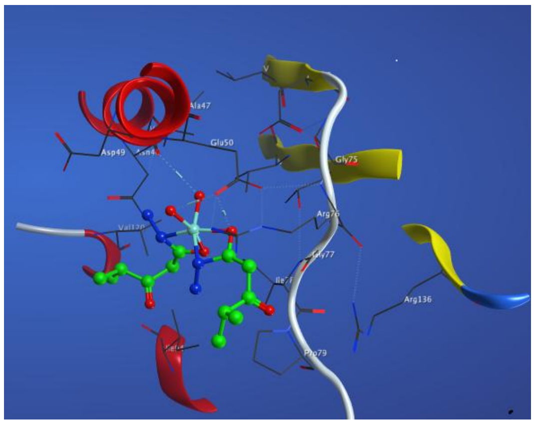 |
| C3 | 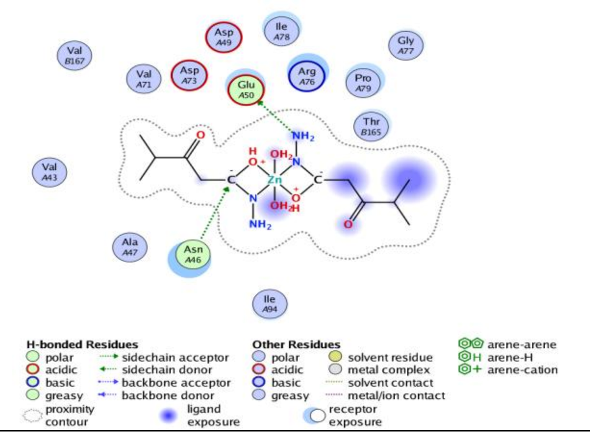 | 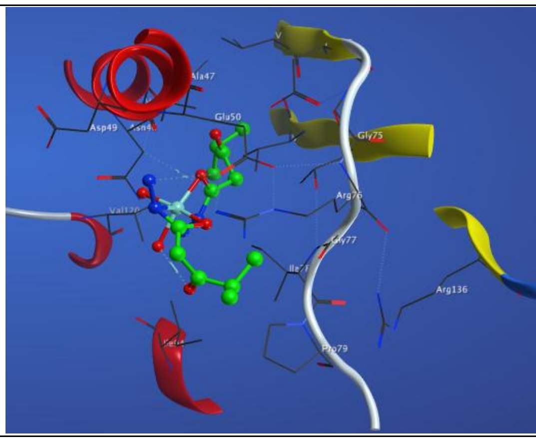 |

| | | |
|---|---|---|
| C7 | 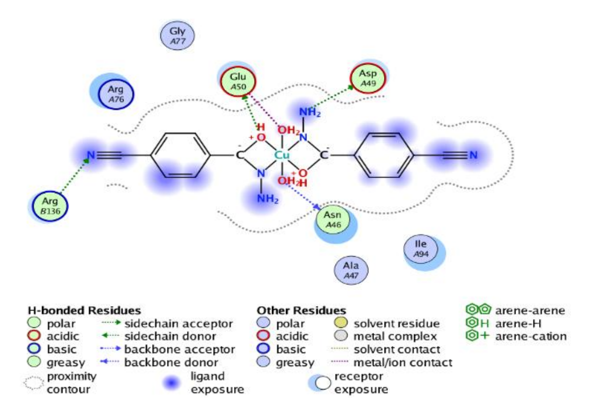 | 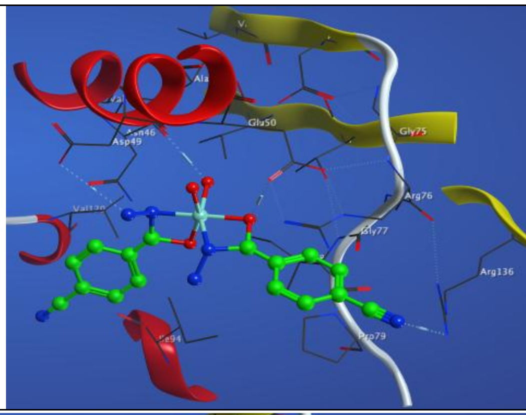 |
| C8 | 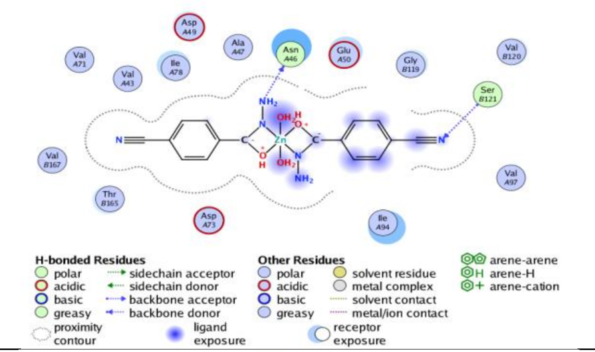 | 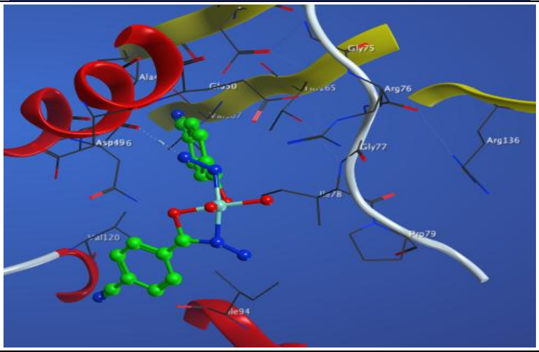 |
| C9 | 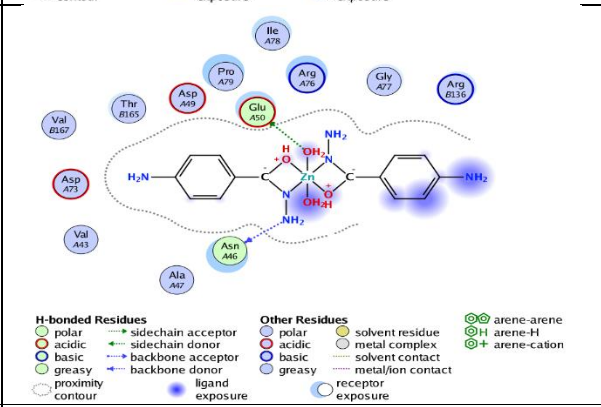 | 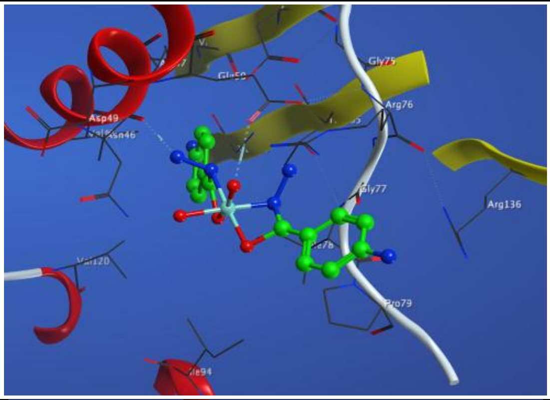 |
| C10 | 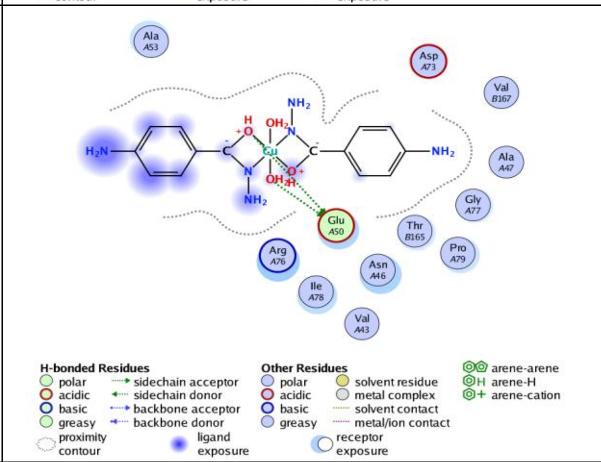 | 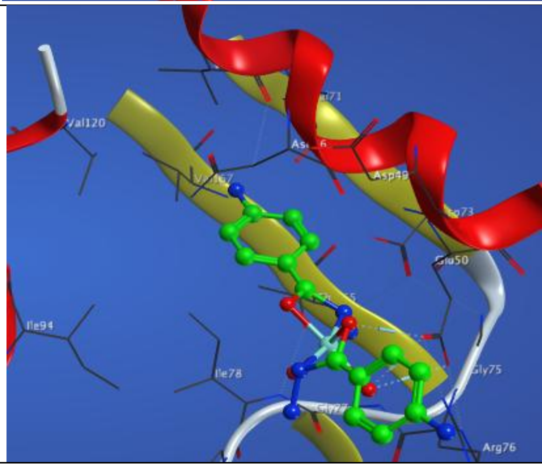 |

| | | |
|---|---|---|
| Ciprofloxacin | 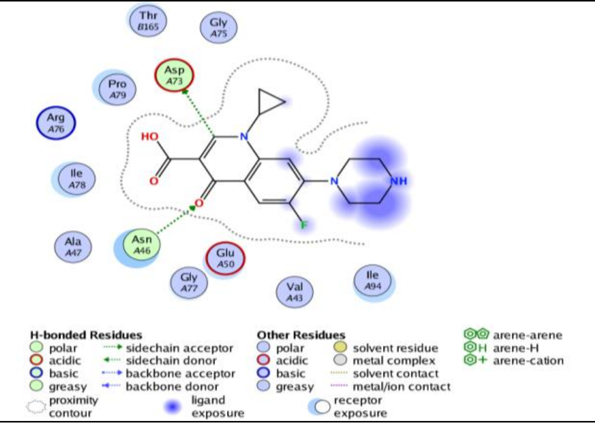 | 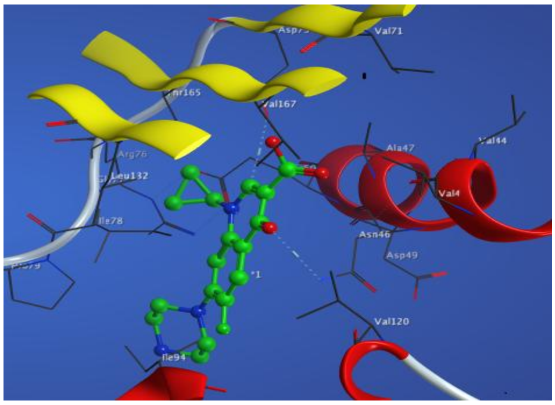 |
| Penicillin | 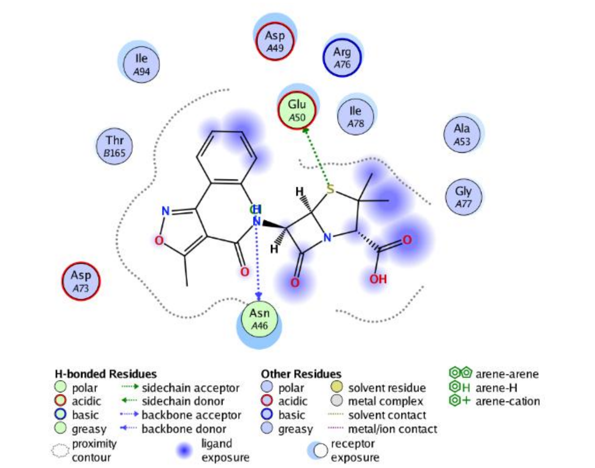 | 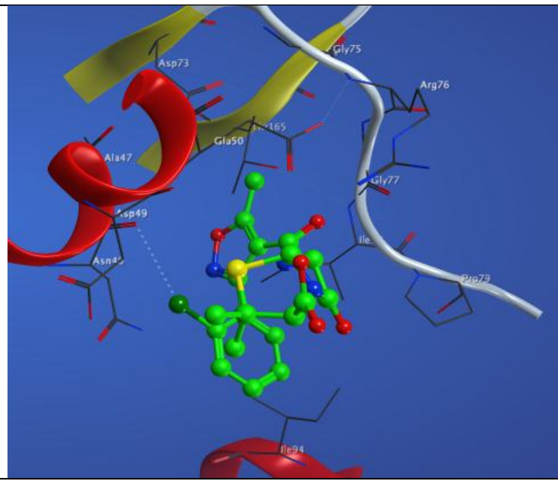 |

**Fig 5:** Interaction diagrams in two- and three-dimensions of complexes and standard drugs with *E.coli* (6F86)

The BE of the complexes with 4URO receptor are ordered as: C7 (-5.811 kcal/mol) > C10 (-5.519 kcal/mol) > C8 (-5.510 kcal/mol) > C3 (-5.160 kcal/mol) > C2 (-5.077 kcal/mol) > C9 (-4.790 kcal/mol), while 5.901 and -5.858 kcal/mol are calculated for penicillin and ciprofloxacin, respectively. This also shows that C7 and C10 have strong binding interactions with the 4URO receptor. Docking simulation shows that C7 interacts with ASPA57 and ASPA57 of the receptor through its oxygen atom of a coordinated water molecule, carbonyl oxygen coordinated to the metal ion with ASNA54, and cyano nitrogen atom with ARGB144 via hydrogen bonding. C10 interacts with GLUA58, ASNA54 and ASPA57 through its oxygen atom of a coordinated water molecule, and GLUA58 through carbonyl oxygen coordinated to the metal ion via hydrogen bonding. Similarly, C2 interacts with ARG84, GLU58 and ASP57 via carbonyl oxygen coordinated to the metal ion and amino nitrogen through hydrogen bonding, whereas C3 only interacts with GLU58 of the receptor through its oxygen atom of a coordinated water molecule. C8 interacts through carbonyl oxygen coordinated to the metal ion and oxygen atom of a coordinated water molecule with GLUA58 via hydrogen bonding interaction, and also to the amino nitrogen atom with ASNA54 via hydrogen bonding interaction (Figure 6). Ciprofloxacin interacts with GLYA585 of the receptor through its carbonyl oxygen of the carboxyl group, hydroxyl oxygen of the carboxyl group with ASPA81 via hydrogen bonding, while penicillin interacts through carbonyl oxygen with ASNA54, and also with thiazolidine sulfur and ARGA84 via hydrogen bonding. The interactions of the complexes with the receptors (4URO and 6F86) show the prevalence of hydrogen bonding interactions of the complexes with the receptors.

| Molecule | 2-D | 3-D |
|---|---|---|
| **C2** | 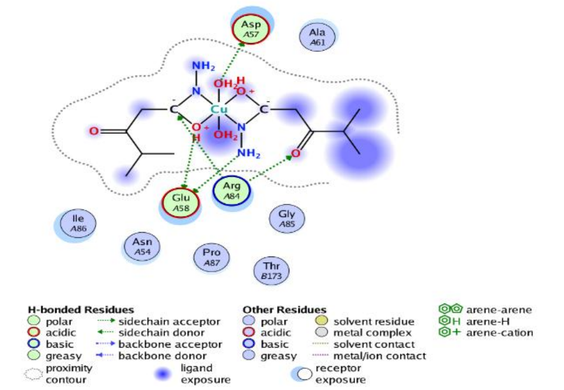 | 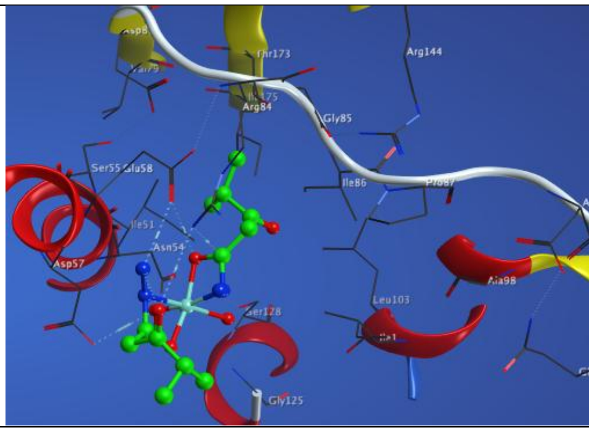 |

<table>
<tr><td>C3</td><td>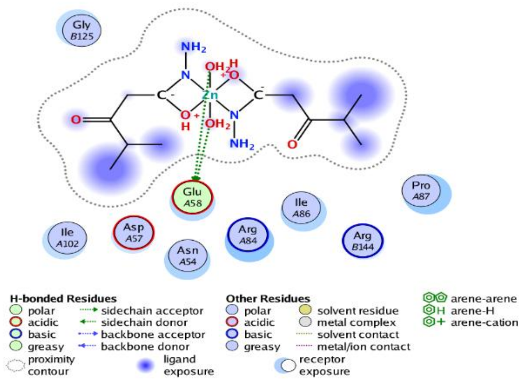
</td><td>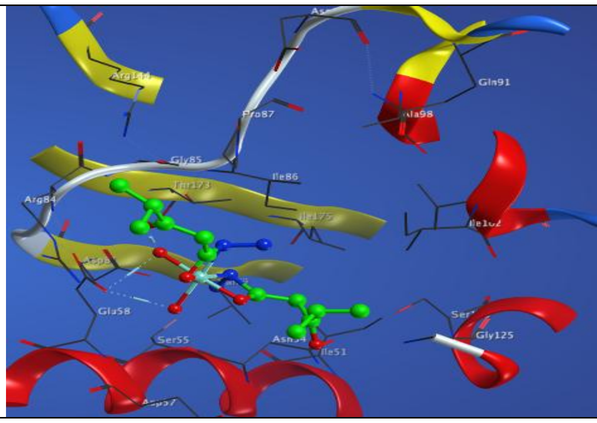
</td></tr>
<tr><td>C7</td><td>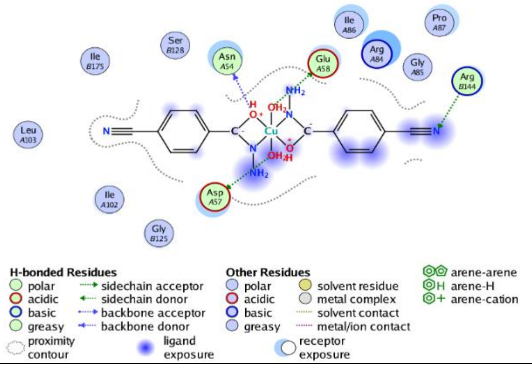
</td><td>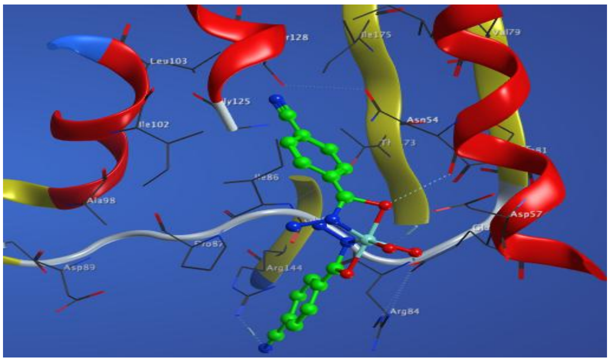
</td></tr>
<tr><td>C8</td><td>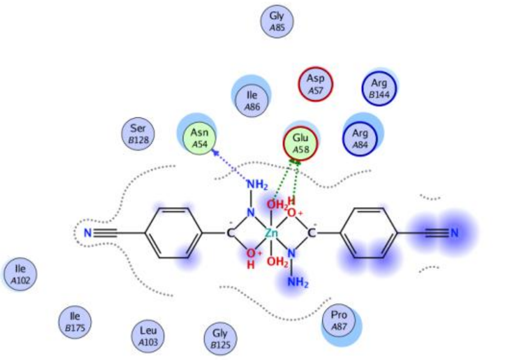
</td><td>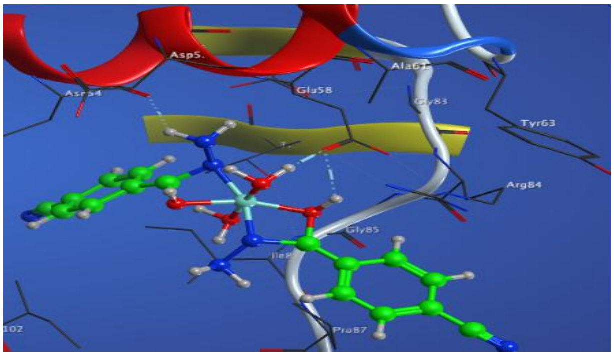
</td></tr>
<tr><td>C9</td><td>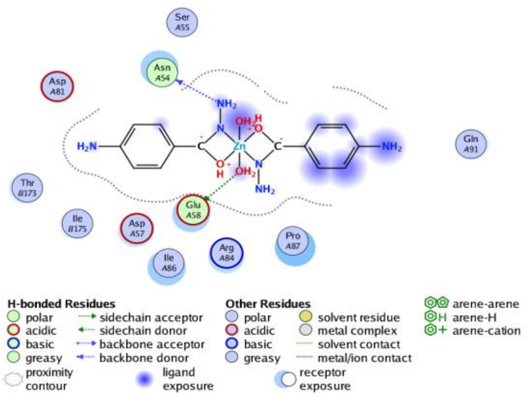
</td><td>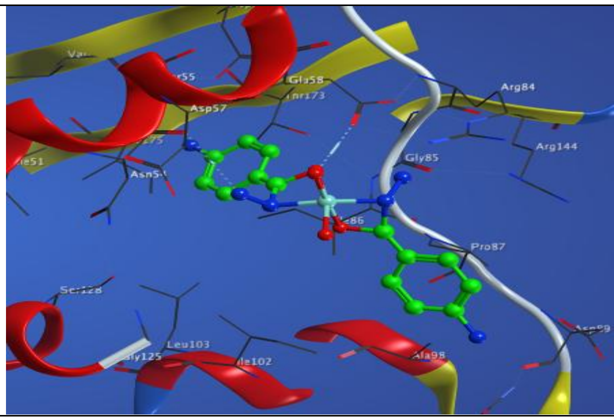
</td></tr>
<tr><td>C10</td><td>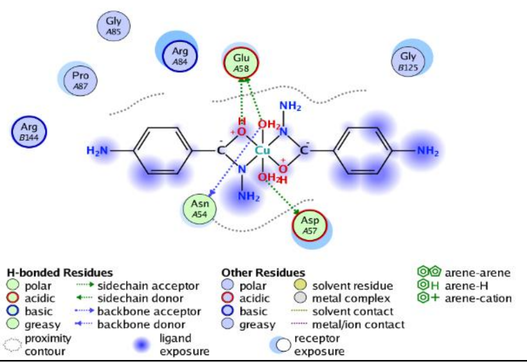
</td><td>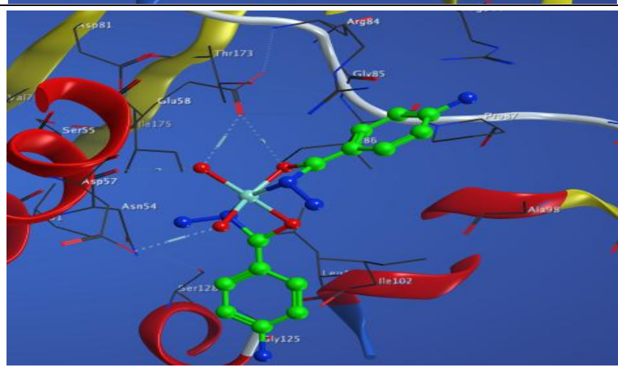
</td></tr>
</table>

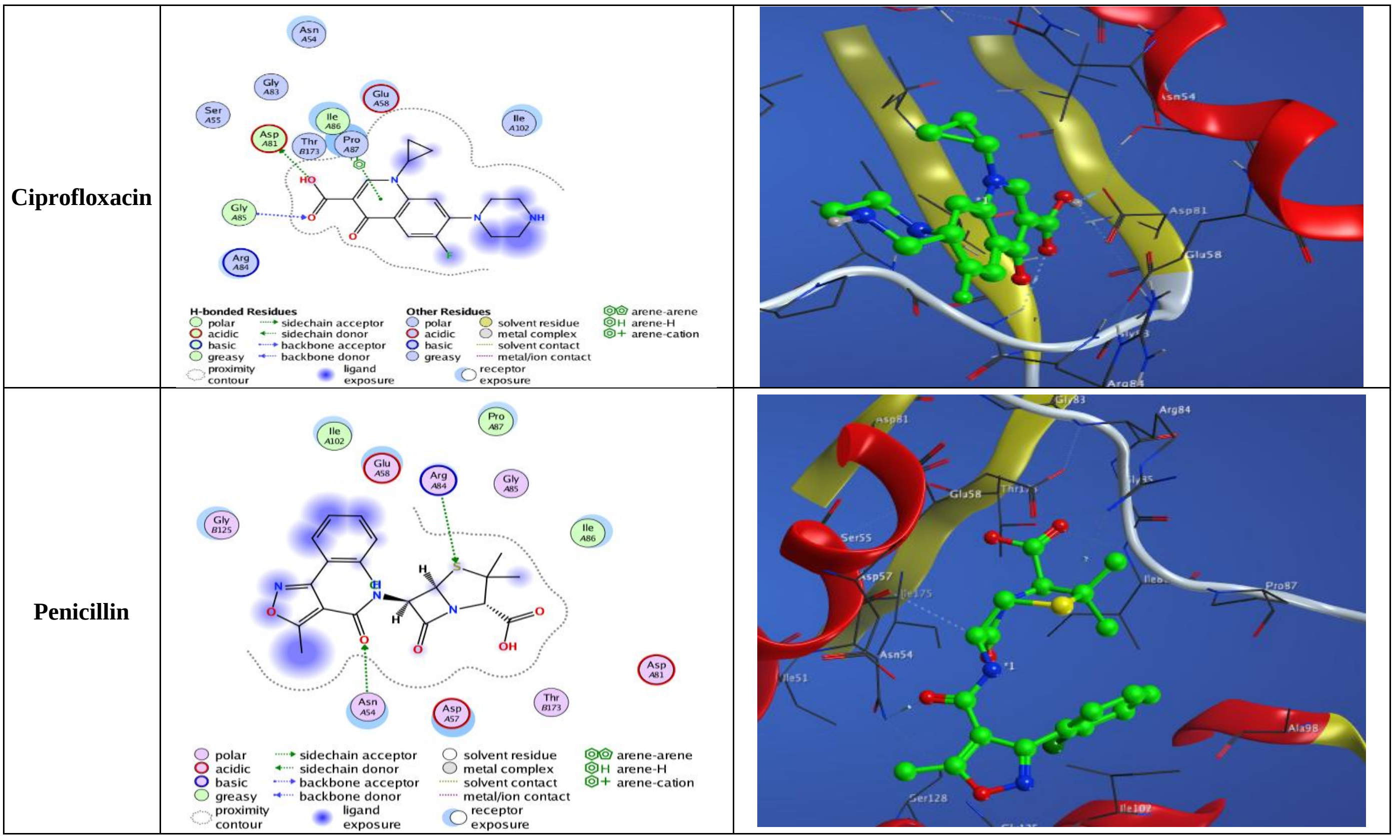


**Fig 6:** Interaction diagrams in two- and three-dimensional of complexes and standard drugs with *S.aureus* (4URO).

**Physicochemical and ADMET Properties of C7, C10 and Standard Drugs**

Physicochemical properties are essential at early stage of the drug development processes for the analysis of the drug-likeness potentially drug molecules. In this work, Lipinski rule of five known as RO5 was used. This hypothesizes that for a candidate molecule to be fitted as an oral drug, it must possess Octanol Water Partition Co-efficient (Log P) ≤ 5, hydrogen bond acceptor (HBA's) ≤ 10, molecular weight (MW) ≤ 500 $gmol^{-1}$, hydrogen bond donor (HBD's) ≤ 5. (Lipinski, 2004). The Log P for C7 and C10 are -0.19 and 0.33; log Kp (cm/s) are -6.38 and -5.94; HBA = 6 and 8; HBD are 4 and 2; TPSA are 113.8 and 109.34, respectively. For ciprofloxacin and penicillin, the Log P are 1.1 and 1.02; log Kp (cm/s) are -9.09 and -8.56; HBA = 5 and 4; HBD are 2 and 2; TPSA are 174.57 and 94.94, respectively, indicating that C7 and C10 as well as the standard drugs do not violate this rule (Table 10 and Figure 7). Also, ADMET profiling was done because many drugs failed during preclinical and clinical stages due to poor and unacceptable ADMET properties (Owonikoko *et al*., 2024) [57]. Therefore, to prevent resource wastage, the Absorption, Distribution, Metabolism, Excretion and Toxicity (ADMET) was carried out to guarantee good efficacy and potency of the candidate drug molecule (Adegbola *et al*., 2021) [58]. In this work, SwissADME web server (http://www.swissadme.ch/index.php) was used to investigate the ADMET properties and the results show C7 and C10 can be absorbed in the intestine, non-inhibitors of Cytochromes P450 enzymes and cannot pass through blood brain barrier (BBB). Thus, C7 and C10 have acceptable ADME properties are shown in Table 10**.**

**Table 10:** Physicochemical and ADMET properties of C7 and C10.

| CmP | MW | HA | AHA | RB | HBA | HBD | MR | TPSA | Log P | log Kp (cm/s) | Lipinski | BS |
|---|---|---|---|---|---|---|---|---|---|---|---|---|
| C7 | 396.93 | 25 | 12 | 2 | 6 | 4 | 102.1 | 113.8 | -0.19 | -6.38 | 0 | 0.56 |
| C10 | 416.92 | 27 | 12 | 2 | 8 | 2 | 102.72 | 109.34 | 0.33 | -5.94 | 0 | 0.56 |
| Ciprofloxacin | 331.34 | 24 | 10 | 3 | 5 | 2 | 95.25 | 74.57 | 1.1 | -9.09 | 0 | 0.55 |
| Penicillin | 320.41 | 22 | 6 | 5 | 4 | 2 | 89.66 | 94.94 | 1.02 | -8.56 | 0 | 0.55 |
| | GI absorption | BBB | Pgp substrate | | CYP1A2 inhibitor | | CYP2C9 inhibitor | | CYP2D6 Inhibitor | | CYP3A4 inhibitor | |
| C7 | High | No | Yes | | No | | No | | No | | No | |
| C10 | High | No | Yes | | No | | No | | No | | No | |
| Ciprofloxacin | High | No | Yes | | No | | No | | No | | No | |
| Penicillin | High | No | Yes | | No | | No | | No | | No | |

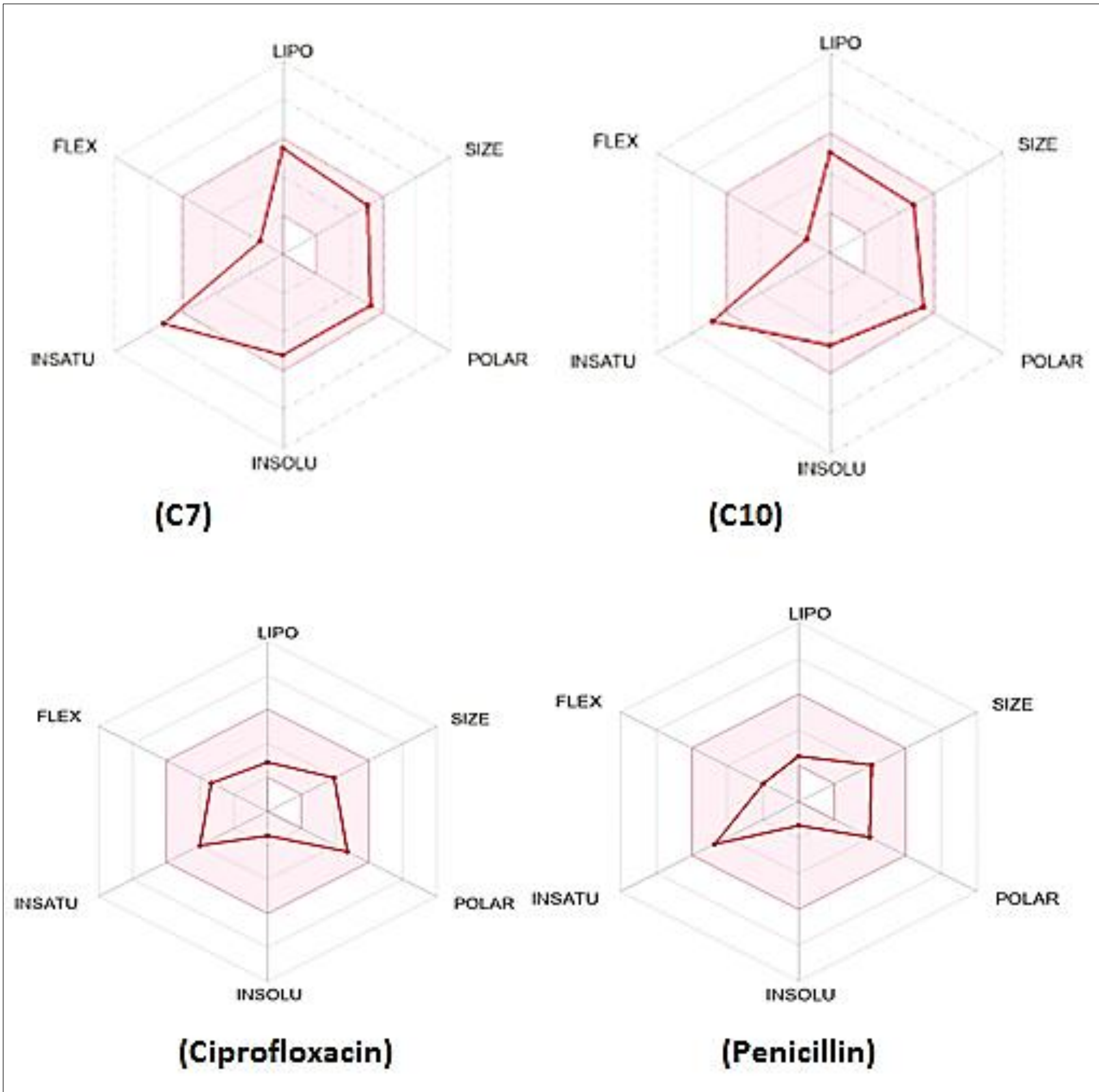


**Fig 7:** The bioavailability radar for the C7, C10 and standard drugs

## Conclusion

This detailed investigation utilized sophisticated computational methods to explore the structural, electronic, spectroscopic, and antimicrobial characteristics of transition metal (II) complexes (Co(II), Mn(II), Cu(II), and Zn(II)) interacting with hydrazide ligands (IBAH, 4-ABAH, and 4-CBAH).

The results offer valuable insights into the coordination chemistry and potential biological functions of these complexes, narrowing the divide between theoretical models and empirical findings. DFT calculations conducted at the B3LYP/6-31G** level confirmed that all complexes adopt octahedral geometries, with optimized bond lengths and angles in agreement with experimental observations. The DFT calculations agreed with the experimental spectroscopic (IR and Electronic) data; thus supporting the octahedral geometries for the M(II) complexes. Molecular docking simulation against Staphylococcus aureus (PDB: 4URO) and Escherichia coli (PDB: 6F86) exhibited strong binding affinities for specific complexes. The Cu(II)-4-CBAH (C7) and Cu(II)-4-ABAH (C10) complexes, in particular, demonstrated binding energy with the receptors comparable to conventional antibiotics (ciprofloxacin and penicillin), which closely aligned with their enhanced *in vitro* antibacterial performance against *E. coli and S. aureus*.

## Reference

1. Rex JH, Lynch HF, Cohen IG, Darrow JJ, Outterson K. Designing Development Programs for Non-Traditional Antibacterial Agents. SSRN Electronic Journal. 2019.
2. Coates AR, Halls G, Hu Y. Novel classes of antibiotics or more of the same? Br J Pharmacol. 2011;163(1):184-94.
3. Popiołek Ł, Biernasiuk A, Berecka A, Gumieniczek A, Malm A, Wujec M. New hydrazide-hydrazones of isonicotinic acid: synthesis, lipophilicity and *in vitro* antimicrobial screening. Chem Biol Drug Des. 2018;91(4):915-23.
4. Belkheiri N, Bouguerne B, Bedos-Belval F, Duran H, Bernis C, Salvayre R, *et al*. Synthesis and antioxidant activity evaluation of a syringic hydrazones family. Eur J Med Chem. 2010;45(7):3019-26.
5. Tolan DA, Kashar TI, Yoshizawa K, El-Nahas AM. Synthesis, spectral characterization, density functional theory studies, and biological screening of some transition metal complexes of a novel hydrazide-hydrazone ligand of isonicotinic acid. Appl Organomet Chem. 2021, 35(6).
6. Vicini P, Incerti M, Doytchinova IA, La Colla P, Busonera B, Loddo R. Synthesis and antiproliferative activity of benzo[d]isothiazole hydrazones. Eur J Med Chem. 2006;41(5):624-632.

7. Ajani OO, Obafemi CA, Nwinyi OC, Akinpelu DA. Microwave assisted synthesis and antimicrobial activity of. 2-quinoxalinone-3-hydrazone derivatives. Bioorg Med Chem. 2010;18(1):214-221.
8. Angelova VT, Valcheva V, Vassilev NG, Buyukliev R, Momekov G, Dimitrov I, *et al*. Antimycobacterial activity of novel hydrazide-hydrazone derivatives with. 2 H -chromene and coumarin scaffold. Bioorg Med Chem Lett. 2017;27(2):223-7.
9. Kumar D, Maruthi Kumar N, Ghosh S, Shah K. Novel bis(indolyl)hydrazide-hydrazones as potent cytotoxic agents. Bioorg Med Chem Lett. 2012;22(1):212-215.
10. Manna K, Agrawal YK. Design, synthesis, and antitubercular evaluation of novel series of 3-benzofuran-5-aryl-1-pyrazolyl-pyridylmethanone and 3-benzofuran-5-aryl-1-pyrazolylcarbonyl-4-oxo-naphthyridin analogs. Eur J Med Chem. 2010;45(9):3831-3189. Available from: https://linkinghub.elsevier.com/retrieve/pii/S0223523410003752
11. Soliman SM, Elsilk SE. Synthesis, X-ray structure, DFT and antimicrobial studies of Ag(I) complexes with nicotinic acid derivatives. J Photochem Photobiol B. 2018;187:48-53.
12. Emam SM, Tolan DA, El-Nahas AM. Synthesis, structural, spectroscopic, and thermal studies of some transition-metal complexes of a ligand containing the amino mercapto triazole moiety. Appl Organomet Chem. 2020, 34(5).
13. Bagchi A, Mukherjee P, Raha A. a Review on Transition Metal Complex-Mordern Weapon in Medicine International Journal of Recent Advances in Pharmaceutical Research a Review on Transition Metal Complex-Mordern Weapon in Medicine. Bagchi *Et al* Int J Recent Adv Pharm Res. 2015;5(3):171-80.
14. Takaya J. Catalysis using transition metal complexes featuring main group metal and metalloid compounds as supporting ligands. Chem Sci. 2021;12(6):1964-81. Available from: https://xlink.rsc.org/?DOI=D0SC04238B
15. Monro S, Colón KL, Yin H, Roque J, Konda P, Gujar S, *et al*. Transition Metal Complexes and Photodynamic Therapy from a Tumor-Centered Approach: Challenges, Opportunities, and Highlights from the Development of TLD1433. Chem Rev. 2019;119(2):797-828. Available from: https://pubs.acs.org/doi/10.1021/acs.chemrev.8b00211
16. Zhang P, Sadler PJ. Redox-Active Metal Complexes for Anticancer Therapy. Eur J Inorg Chem. 2017;2017(12):1541-8. Available from: https://chemistry-europe.onlinelibrary.wiley.com/doi/10.1002/ejic.201600908
17. Joseph J, Nagashri K, Rani GAB. Synthesis, characterization and antimicrobial activities of copper complexes derived from 4-aminoantipyrine derivatives. Journal of Saudi Chemical Society. 2013;17(3):285-94.
18. Singh AK, Pandey OP, Sengupta SK. Synthesis, spectral characterization and biological activity of zinc(II) complexes with 3-substituted phenyl-4-amino-5-hydrazino-1,. 2, 4-triazole Schiff bases. Spectrochim Acta A Mol Biomol Spectrosc. 2011;
19. Salawu, OW., Eneji, IS., & Iornumbe EN. Synthesis and Characterization of. 2-Ethoxy Isobutryl Acid Hydrazide and. 2-Ethoxy Isobutryl Aceto Hydrazone and Its Metal Complexes with Co(II), Ni(II) and Cu(II). Chemistry and Materials Research. 2015;7:No.4, 53-54.
20. Orhan Puskullu M, Tekiner B, Suzen S. Recent Studies of Antioxidant Quinoline Derivatives. Mini Rev Med Chem. 2013;13(3):365-72.
21. Kumar S, Bawa S, Drabu S, Kumar R, Gupta H. Biological Activities of Pyrazoline Derivatives -A Recent Development. Recent Pat Antiinfect Drug Discov. 2009;4(3):154-63.
22. Narang R, Narasimhan B, Sharma S. A Review on Biological Activities and Chemical Synthesis of Hydrazide Derivatives. Curr Med Chem. 2012;19(4):569-612.
23. Nwambueze JN, Salawu OW. Complexes Of Co(II) and Mn(II) Sulphate With Keto And Enolforms Forms of Isobutryl Acetic Acid, 4-Amino Benzoic Acid and 4-Cyano Benzoic Acid Hydrazide. The International Journal Research Publications; Research Journal of Science & IT Management. 2012;1(9):28-35.
24. Nwambueze JN, Salawu OW. Complexes Of Ni(II) and Cu(II) Sulphate With Keto And Enolforms Forms of Isobutryl Acetic Acid, 4-Amino Benzoic Acid and 4-Cyano Benzoic Acid Hydrazide. Advance in Pure and Applied Chemistry (APAC). 2012;1(2):4048.
25. Nwambueze JN, Salawu OW. Complexes Of Zn(II) And Vo(IV) Sulphate With Keto And Enolforms of Isobutryl Acetic Acid, 4-Amino Benzoic Acid nd 4-Cyano Benzoic Acid Hydrazide. Advance in Pure and Applied Chemistry. 2012;1(2):20-30.
26. Shevyrin V, Melkozerov V, Nevero A, Eltsov O, Baranovsky A, Shafran Y. Synthetic cannabinoids as designer drugs: New representatives of indol-3-carboxylates series and indazole-3-carboxylates as novel group of cannabinoids. Identification and analytical data. Forensic Sci Int. 2014;244:263-275.
27. Kirste B. Applications of Density Functional Theory to Theoretical Organic Chemistry. Chem Sci J. 2016, 7(2).
28. Adekunle FAO, Semire B, Odunola OA. Synthesis, characterization, and quantum chemical studies of Ru(phen)2Cl2.2H2O and Ru(bipy)2Cl2.2H2O With. 2,6-diacetylpyridinedihydrazone. Synthesis and Reactivity in Inorganic, Metal-Organic and Nano-Metal Chemistry. 2015;45(8):1102-1107.
29. Semire B, Mutiu O, Oyebamiji AK. DFT and AB INITIO Methods on NMR, IR and Reactivity Indices of Indol-3-Carboxylate and Indazole-3-Carboxylate Derivatives of Cannabinoids: Comparative Study. 2017. Available from: www.SID.ir
30. Paul MKr, Dilipkumar Singh Y, Bedamani Singh N, Sarkar U. Emissive bis-salicylaldiminato Schiff base ligands and their zinc(II) complexes: Synthesis, photophysical properties, mesomorphism and DFT studies. J Mol Struct. 2015;1081:316-328.
31. M. Abd El-Lateef H, M. Ali A, M. Khalaf M, Abdou A. New Fe(III), Co(II), Ni(II), Cu(II), and Zn(II) mixed-ligand complexes: stractural, DFT, biological, and molecular docking studies. Bull Chem Soc Ethiop. 2024;38(2):397-416. Available from: https://www.ajol.info/index.php/bcse/article/view/263222
32. Shaaban S, Abdou A, Alhamzani AG, Abou-Krisha MM, Al-Qudah MA, Alaasar M, *et al*. Synthesis and in Silico Investigation of Organoselenium-Clubbed Schiff Bases as Potential Mpro Inhibitors for the SARS-CoV-2 Replication. Life. 2023;13(4):912.
33. Shaaban S, Al-Faiyz YS, Alsulaim GM, Alaasar M, Amri N, Ba-Ghazal H, *et al*. Synthesis of New

Organoselenium-Based Succinanilic and Maleanilic Derivatives and In Silico Studies as Possible SARS-CoV-2 Main Protease Inhibitors. Inorganics (Basel). 2023;11(8):321.
34. Suleman VT, Al-Daher AGM. Synthesis, Characterization, Density Functional Theory Studies and Antioxidant Activity of Novel Hydrazone Ligands and their Metal Complexes. Oriental Journal of Chemistry. 2023;39(6):1629-1642.
35. Ramadan RM, El-Medani SM, Makhlouf A, Moustafa H, Afifi MA, Haukka M, *et al*. Spectroscopic, density functional theory, nonlinear optical properties and *in vitro* biological studies of Co(II), Ni(II), and Cu(II) complexes of hydrazide Schiff base derivatives. Appl Organomet Chem. 2021, 35(7).
36. Alkurdi A, Aljahdali M, Alshehri A. Study of Synthesis, Characterization, DFT, and *in vitro* Biological Activity of Cu(II), Co(II), and Fe(II) Metal Complexes Based on Heterocyclic Azo Pyrazole Dye Ligand. J Chem, 2022.
37. El-Remaily MAEAAA, El-Dabea T, El-Khatib RM, Abdou A, El Hamd MA, Abu-Dief AM. Efficiency and development of guanidine chelate catalysts for rapid and green synthesis of 7-amino-4,5-dihydro-tetrazolo [1,5- *a* ]pyrimidine-6-carbonitrile derivatives supported by density functional theory (DFT) studies. Appl Organomet Chem. 2023, 37(11).
38. Abdel-Rhman MH, El-Asmy AA, Ibrahim R, Hosny NM. New Schiff base ligand and some of its coordination compounds: Synthesis, spectral, molecular modeling and biological studies. J Mol Struct. 2023;1279:135023.
39. Latif MA, Ahmed T, Hossain MdS, Chaki BM, Abdou A, Kudrat-E-Zahan Md. Synthesis, Spectroscopic Characterization, DFT Calculations, Antibacterial Activity, and Molecular Docking Analysis of Ni(II), Zn(II), Sb(III), and U(VI) Metal Complexes Derived from a Nitrogen-Sulfur Schiff Base. Russ J Gen Chem. 2023;93(2):389-397.
40. Mohapatra RK, Mahal A, Ansari A, Kumar M, Guru JP, Sarangi AK, *et al*. Comparison of the binding energies of approved mpox drugs and phytochemicals through molecular docking, molecular dynamics simulation, and ADMET studies: An in silico approach. J Biosaf Biosecur. 2023;5(3):118-32.
41. Hosny NM, Samir G, Abdel-Rhman MH. N′-(Furan-2-ylmethylene)-2-hydroxybenzohydrazide and its metal complexes: synthesis, spectroscopic investigations, DFT calculations and cytotoxicity profiling. BMC Chem. 2024;18(1):1-17. Available from: https://doi.org/10.1186/s13065-023-01098-8
42. Godwini R, Monicka JC, Victoria SG. Analyses on the reactivity, topology and bioactivity of Fluazinam using density functional theory. Chemical Physics Impact. 2023;7:100309.
43. Kikuchi O. Systematic QSAR Procedures with Quantum Chemical Descriptors. Quantitative Structure-Activity Relationships 1987;6(4):179-84.
44. Housecroft CE, Sharpe AG. Inorganic chemistry (4th ed.). Pearson Education Limited. 2008.
45. Pauling L. The Nature of the Chemical Bond and the Structure of Molecules and Crystals: An Introduction to Modern Structural Chemistry. Cornell University Press, Ithaca, New York 1960;3rd:10-13.
46. Chattaraj PK, Giri S, Duley S. Update. 2 of: Electrophilicity Index. Chem Rev. 2011;111(2):PR43-75.
47. El-Remaily MAEAAA, Elhady O, Abdou A, Alhashmialameer D, Eskander TNA, Abu-Dief AM. Development of new. 2-(Benzothiazol-2-ylimino)-2,3-dihydro-1H-imidazol-4-ol complexes as a robust catalysts for synthesis of thiazole 6-carbonitrile derivatives supported by DFT studies. J Mol Struct. 2023;1292:136188.
48. Olanrewaju AA, Oke DG, Adekunle DO, Adeleke OA, Akinola OT, Emmanuel A V., *et al*. Synthesis, *in-vitro* and in-silico antibacterial and computational studies of selected thiosemicarbazone-benzaldehyde derivatives as potential antibiotics. SN Appl Sci. 2023, 5(8).
49. Pérez P, Domingo LR, Aizman A, Contreras R. Chapter 9 The electrophilicity index in organic chemistry. Theoretical and Computational Chemistry. 2007;19:139-201.
50. Merrick JP, Moran D, Radom L. An Evaluation of Harmonic Vibrational Frequency Scale Factors. J Phys Chem A. 2007;111(45):11683-700.
51. Bello I.A, Semire B. Theoretical Study on Structural and Electronic Properties of 4-[(E)-[4-(trifloromethyl)-1,3-benzothiazol-2-yl]azo]naphthalen-1-ol and 1-[(E)-[4-(trifloromethyl)-1,3-benzothiazol-2-yl]azo]naphthalen-2-ol using Density Functional Theory (DFT). International Journal of Physical Sciences. 2013;8(29):1494-505.
52. Adekunle FAO, Semire B, Odunola OA. Synthesis, characterization and quantum chemical studies of some Co(II) and Cu(II) complexes of acetoacetic acid hydrazide. Asian Journal of Chemistry. 2013;25(13):7371-6.
53. Shakdofa MME, Morsy NA, Rasras AJ, Al-Hakimi AN, Shakdofa AME. Synthesis, characterization, and density functional theory studies of hydrazone-oxime ligand derived from. 2,4,6-trichlorophenyl hydrazine and its metal complexes searching for new antimicrobial drugs. Appl Organomet Chem. 2021;35(2):1-19.
54. Preethi V, Vijukumar VG, AnilaRaj S, Vidya VG. Synthesis, characterization, DFT studies and evaluation of the potential anti-tumour activity of nicotinic hydrazide based Schiff base using *in vitro* and molecular docking techniques. Heliyon. 2024, 10(9).
55. Elkanzi NAA, Hrichi H, Salah H, Albqmi M, M.Ali A, Abdou A. Synthesis, physicochemical properties, biological, molecular docking and DFT investigation of Fe(III), Co(II), Ni(II), Cu(II) and Zn(II) complexes of the 4-[(5-oxo-4,5-dihydro-1,3-thiazol-2-yl)hydrazono]methyl}phenyl 4-methylbenzenesulfonate Schiff-base ligand. Polyhedron. 2023;230:116219.
56. Wahab OO, Waziri I, Oselusi SO. Zinc (II) complex of (Z) -4- ((4-nitrophenyl*et al* amino*et al* pent-3-en-2-one, a potential antimicrobial agent: Synthesis, characterization, electrochemical, antimicrobial, DFT and docking studies. 2022;(Ii):1-20.
57. Owonikoko AD, Sodamade A, Modupe Olatunde A, Odoje OF, Semire B. In silico Identification of bioactive compounds from Chasmanthera dependens and Carissa edulis as potential inhibitors of Carbonic anhydrases (CAs) receptors using a target-based drug design approach. 2024. Available from: www.ijnrd.org
58. Adegbola PI, Semire B, Fadahunsi OS, Adegoke AE. Molecular docking and ADMET studies of Allium cepa, Azadirachta indica and Xylopia aethiopica isolates as potential anti-viral drugs for Covid-19. Virusdisease. 2021;32(1):85-97.